J. Fluid Mech. (1996), *vol.* 312, *pp.* 1–37

Turbulent boundary-layer flow over fixed aerodynamically rough two-dimensional sinusoidal waves

By WANMIN GONG[1], PETER A. TAYLOR[2] AND ANDREAS DÖRNBRACK[3]

[1] ARQI, Atmospheric Environment Service, 4905, Dufferin St., Downsview, Ontario, Canada, M3H 5T4

[2] Department of Earth and Atmospheric Science, York University, North York, Ontario, Canada, M3J 1P3

[3] Institute of Atmospheric Physics, DLR, D-82230, Oberpfaffenhofen, Germany

(Received 15 June 1994 and in revised form 14 October 1995)

Results from a wind tunnel study of aerodynamically rough turbulent boundary-layer flow over a sinusoidal surface are presented. The waves had a maximum slope (ak) of 0.5 and two surface roughnesses were used. For the relatively rough surface the flow separated in the wave troughs while for the relatively smooth surface it generally remained attached. Over the relatively smooth-surfaced waves an organized secondary flow developed, consisting of vortex pairs of a scale comparable to the boundary-layer depth and aligned with the mean flow. Large-eddy simulation studies model the flows well and provide supporting evidence for the existence of this secondary flow.

1. Introduction

There have been numerous studies of turbulent boundary-layer flow over topography conducted over the years, many concerned with stably stratified flow and lee waves, but others focusing on neutrally stratified flow. Reviews by Taylor, Mason & Bradley (1987), Finnigan (1988) and Carruthers & Hunt (1990) deal with this aspect, and it is also the topic for a chapter in the recent book by Kaimal & Finnigan (1994). In addition to considering the velocity perturbations induced by topography, some studies have also considered the pressure distribution on the underlying surface and the related form drag. The form drag is of particular interest in attempting to parameterize the effects of small-scale topography for large-scale atmospheric flow models, as illustrated by the work of Taylor, Sykes & Mason (1989) and Wood & Mason (1993). Furthermore the pressure distribution is critical to the wind wave generation process. This was the focus of the early experimental studies of Stanton, Marshall & Houghton (1932) and Motzfeld (1937), and several other contributions (e.g. Kendall 1970) have been motivated, at least in part, by an interest in wind wave generation. Perhaps partly because of this, all of the previous wind tunnel and water channel studies that we are aware of, including those by the University of Illinois group (see for example Buckles, Hanratty & Adrian 1984; Abrahams & Hanratty 1985; and Kuzan, Hanratty & Adrian 1989), have been for flow over waves with aerodynamically smooth surfaces, for which there will be some Reynolds number dependence. The Reynolds number will influence the wave slope required to cause flow separation (see Zilker, Cook & Hanratty 1977) and the variation of local surface shear stress between trough and crest

may cause the viscous sub-layer thickness and the 'effective roughness length' (see Garratt 1992, p. 87) to vary along the length of a wave. To the best of our knowledge the wind tunnel study reported here is the first to use aerodynamically rough surfaces.

Here we present new wind tunnel measurements and large-eddy simulation (LES) results. The measurements include the discovery of a secondary flow which developed in one of our wind tunnel flow cases. Similar, though not identical, features were present in our large-eddy simulations. All of the flows considered are neutrally stratified and we will not discuss situations in which internal gravity waves would be generated. A preliminary description of the experimental results was presented at a 1989 ALPEX meeting in Garmisch-Partenkirchen and at a 1990 Euromech colloquium in Bologna (see Hunt *et al.* 1991). Attempts to reproduce our observed mean flow with models based on solutions of the ensemble-averaged equations are discussed in Taylor *et al.* (1995).

Theoretical models of flow over wavy surfaces include the work of Miles (1957), Townsend (1972), Caponi *et al.* (1982) and others on wind wave generation. Miles' theory is essentially inviscid while Caponi *et al.* consider a laminar viscous flow. Most other models of flow over topography (including Townsend 1972; Taylor 1977*a*; Beljaars, Walmsley & Taylor 1987; Maat & Makin 1992; and Xu & Taylor 1992) use the ensemble-averaged or Reynolds equations for turbulent flow and invoke closure assumptions at some level. As Ayotte, Xu & Taylor (1994) have recently demonstrated, some flow predictions, especially turbulence in the 'outer layer', but also the form drag, can be strongly dependent on the closure used while the overall predictions of mean wind speed variation, at least for low slopes, are relatively insensitive. Several models (e.g. Jackson & Hunt 1975; Beljaars *et al.* 1987) are linearized in wave slope (ak) and formally restricted to waves of low slope, although in practice they are often used for moderate slopes provided that the flow remains attached. With slopes large enough to cause flow separation, local Reynolds-average closure assumptions become rather questionable, because the separated region is often fluctuating in size and the separation itself may well be intermittent. With this caution, we can note that Gent & Taylor (1977) model separated flows, mostly for water waves but including some fixed wave cases. Xu, Ayotte & Taylor (1994) investigate the errors associated with the use of linear models and also present results from an improved version of their nonlinear mixed spectral finite difference (NLMSFD) model.

For flow over an infinite train of two-dimensional sinusoidal waves there are applications to studies of the flow over sand or gravel waves and, allowing for differences in the surface boundary condition, indirect applications to the flow over water waves. Our primary motivation however is that sinusoidal topography represents a canonical, complex terrain situation and thus has an inherent importance in attempts to refine our understanding of turbulent flow in the atmospheric boundary layer.

2. The flow configuration

The flow is neutrally stratified and can be considered as a modification of, or perturbation to, stationary horizontally homogeneous infinitely deep undirectional constant-stress-layer flow above a plane aerodynamically rough surface of uniform roughness, z_0. This basic flow will have a logarithmic mean velocity profile,

$$U = (u_*/\kappa)\ln((z+z_0)/z_0), \tag{1}$$

where u_* is the friction velocity and κ is the von Kármán constant, which we will take as 0.4.

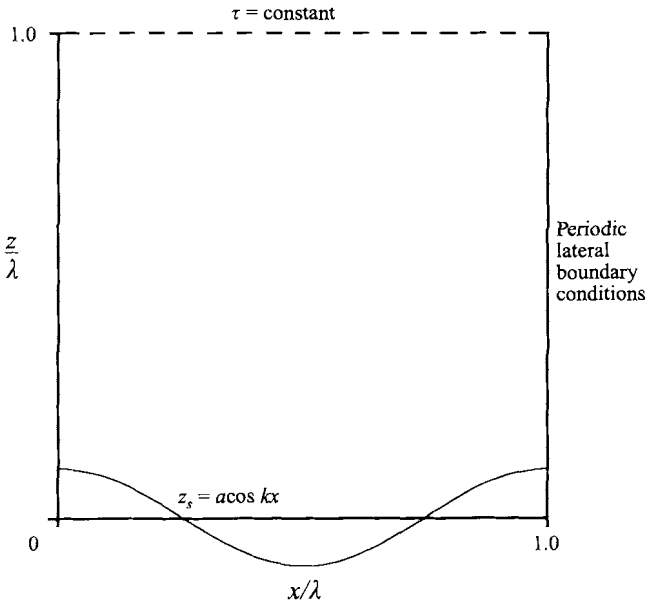

FIGURE 1. Flow over a periodic wavy surface at the bottom of a deep constant-stress turbulent boundary layer.

Let us consider the situation with the plane lower boundary replaced by an infinite periodic wavy surface with elevation,

$$z_s = a\cos kx. \tag{2}$$

The wave crests are perpendicular to the flow direction, a is the wave amplitude, λ is the wavelength and $k = 2\pi/\lambda$ is the wavenumber. The maximum wave slope will be ak. This flow situation is illustrated in figure 1. The topographically induced flow has substantially decayed at $z = \lambda$, and upper boundary conditions can generally be applied at that level. Throughout this paper we will use z' to denote height above the local surface and z to denote height above a plane surface. The flow is assumed to be periodic and can still be a constant-stress layer for horizontal averages over a wavelength. For wavelength averages on horizontal planes with $z > a$ the total wavelength-averaged kinematic shear stress will be

$$-\langle\overline{u'w'}\rangle - \langle UW\rangle = u_*^2, \tag{3}$$

where the upper-case symbols and overbars represent mean quantities (time or ensemble averages), primed quantities are turbulent fluctuations and $\langle\ \rangle$ indicates a wavelength-averaged quantity. As z increases, the mean flow Reynolds stress, $\langle UW\rangle$, will decay and all of the stress will be associated with the turbulent contribution (cf. Taylor *et al.* 1989).

For this ideal Reynolds-number-independent flow, which is one of the situations considered in Taylor (1977*a*) and several other modelling papers, we have just two external parameters defining the flow in a non-dimensional sense. These are the maximum wave slope, ak, and the ratio of wavelength to roughness length λ/z_0. The mean flow, and all integral statistics, are expected to be independent of the cross-stream coordinate, y, and to be periodic in x with wavelength λ.

Unfortunately in all of the laboratory studies of flow over a wavy surface that we are aware of, including our own, the boundary layer is not sufficiently deep to be

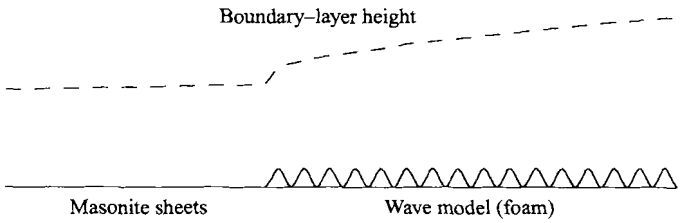

FIGURE 2. Sketch of the wind tunnel arrangement. Vertical scale exaggerated approximately 10×.

considered as a true constant-stress layer up to a depth of $O(\lambda)$, although the flow variations over the waves may be essentially periodic throughout most of the boundary-layer depth. This depth is either still growing slowly at the measurement location or the boundary layer could, in effect, have become part of a two-dimensional channel flow (as in the experiment reported by Buckles *et al.* 1984). In either case the total shear stress will vary with height. In practice this variation is often on a similar scale to the vertical extent of the topographically induced velocity perturbations. The insufficient depth of the boundary layer is a result of experimenters wanting long enough waves in order to make measurements within the 'inner layer', close to the surface, and sufficient waves to ensure a fully developed periodic flow within the boundary layer over the waves. The spatially evolving boundary layer is illustrated in figure 2. At measurement locations over the 10th and 12th waves in our experiments the boundary-layer depth (600 mm) was approximately equal to λ, although at the upstream reference measurement location or in the flow over a flat floor without the wave model present it was rather shallower (100–250 mm). From a theoretical or numerical modelling point of view it is difficult to handle the steadily growing boundary-layer situation since we cannot assume spatially periodic boundary conditions. Most of the numerical results obtained to date are either for the idealized constant-stress layer discussed above or for the horizontally homogeneous (in a wavelength-average sense) planetary boundary layer (e.g. Taylor 1977*b* or Newley 1985). In our LES modelling, we will consider a time-dependent flow, with periodic boundary conditions, initialized with velocity and turbulence characteristics representative of the upstream conditions in the wind tunnel. If we define $T_{ref} = \lambda/U_0$, where U_0 is the free-stream velocity in the wind tunnel, then there will be an approximate equivalence between the wind tunnel flow at distance $n\lambda$ from the start of the wavy surface and the spatially periodic simulated flow after a time nT_{ref}. We will assume this similarity in comparing wind tunnel and LES data.

In comparing results from various models and experiments it is necessary to select a suitable scaling velocity. There are several choices for this: (*a*) a surface friction velocity, u_*; (*b*) a bulk velocity, U_b, based on mass flux and obtained by integration over the depth of a channel, as in Buckles *et al.* 1984; (*c*) an average velocity at some height, often taken to be λ; or (*d*) the free-stream velocity, U_0, if the concept applies. The internal scaling velocity for the LES model that we use is U_b but in the present paper we will generally use U_0 as our scaling velocity since this is unambiguous for our experimental work. In the wind tunnel setting $U_0 \approx U_\lambda$.

3. The wind tunnel, the wave model and the undisturbed flow

The experiment was conducted in the AES (Atmospheric Environment Service, Canada) meteorological wind tunnel, which has a working section of 2.44 m × 1.83 m × 18.29 m ($W \times H \times L$). A detailed description of the wind-tunnel

facility and the basic data acquisition and analysis system is given in Shokr & Teunissen (1988). Velocity measurements were made with both single hot-wire and cross-wire (X) probes while surface pressure measurements were obtained at a series of pressure tappings both in the sidewall of the tunnel (for free-stream pressure variation) and in the lower, wavy boundary, over the first and the tenth waves, where access to the model was relatively easy. There were 26 pressure tappings over one wavelength with higher resolution over the steepest parts of the wave slope to assist in the accurate determination of form drag. A scanivalve multiplexer was used to sequentially direct signals from all pressure ports to a single electronic manometer.

The wave model was made from high-density polyurethane foam. It consisted of sixteen sinusoidal waves with wavelength $\lambda = 609.6$ mm and trough to crest height $2a = 96.5$ mm, which gave a maximum surface slope $ak = 0.50$. For the natural foam surface, which was relatively, though not aerodynamically, smooth, velocity profile measurements over a plane surface gave $z_0 = 0.03$ mm and $\lambda/z_0 = 2 \times 10^4$ while with a carpet cover (relatively, and aerodynamically, 'rough'), $z_0 = 0.4$ mm and $\lambda/z_0 = 1.5 \times 10^3$. The wave model was placed with its leading edge at a distance $x = 6.1$ m downstream from a honeycomb located at the downstream end of the contraction region and joined (flush) with Masonite (hardboard) sheets upstream. These sheets were shown to have approximately the same surface roughness length as the foam. In the rough case, the waves as well as the upstream flat floor were covered with carpet of uniform (5 mm) thickness with no change caused to the wave topography.

To obtain the characteristics of the undisturbed flow for the relatively smooth surface case, measurements were first carried out in the tunnel without the wave model. In this case, the entire wind tunnel floor was covered with Masonite sheets and an approximate zero longitudinal pressure gradient was obtained over the major test section ($x > 0$) by adjustment of the tunnel roof panels. Vertical profiles of mean wind speed U and turbulence components $\sigma_u, \sigma_v, \sigma_w$ and $(-\overline{u'w'})$ were taken at three positions along the central plane of the wind tunnel, assuming the flow to be two-dimensional. The free-stream velocity, U_0, approximately 1 m above the floor of the tunnel, was set to about 10 m s^{-1} during the measurements. Here, and in the discussion of flow over the wavy surface, we will present the turbulence data after rotation into streamline coordinates (s, y, n). Thus σ_u is used to indicate $(\overline{u_s' u_s'})^{1/2}$, etc. A semi-logarithmic plot of time-mean velocity profiles, figure 3(*a*), gives essentially the same roughness length (0.03 mm) at the three measurement positions. The friction velocity u_* can be evaluated from the profiles, assuming a logarithmic profile, (1). Results for u_*, based on the slope of the lower portion of the profiles ($1 < z' < 100$ mm) on a log-linear plot, range from 0.45 m s^{-1} at $x = 6.7$ m to 0.41 m s^{-1} at $x = 14.0$ m due to the growth of boundary layer. The boundary-layer depth was about 200 mm at the first downstream position and about 250 mm at the last position. The flow had a roughness Reynolds number $R(= u_* z_0/\nu)$ of about 0.8, and was therefore not quite fully aerodynamically rough ($R > 2.5$, cf. Sutton 1953, p. 82). However it will differ from fully aerodynamically rough flow only very close to the surface, and the main body of the flow should still be virtually independent of Reynolds number.

Turbulence profiles σ_u, σ_v and σ_w, at the downstream position ($x = 14$ m), are plotted in figure 3(*c*), while in figure 3(*b*) we show the shear stress profiles at three measurement locations. The σ and $-\overline{u'w'}$ profiles are approximately constant over the lowest one third of the boundary layer and decrease above. Near-surface ratios $(\sigma_u, \sigma_v, \sigma_w)/u_*$ have values of approximately (2.2, 1.3, 1.0) in reasonable accord with those obtained in other wind tunnel studies by, for example, Gong & Ibbetson (1989) of (2.2, 1.5, 1.0) or Counihan (1975) of (2.5, 1.9, 1.3). Scaling to U_0 gives $(\sigma_u, \sigma_v, \sigma_w)/U_0 =$

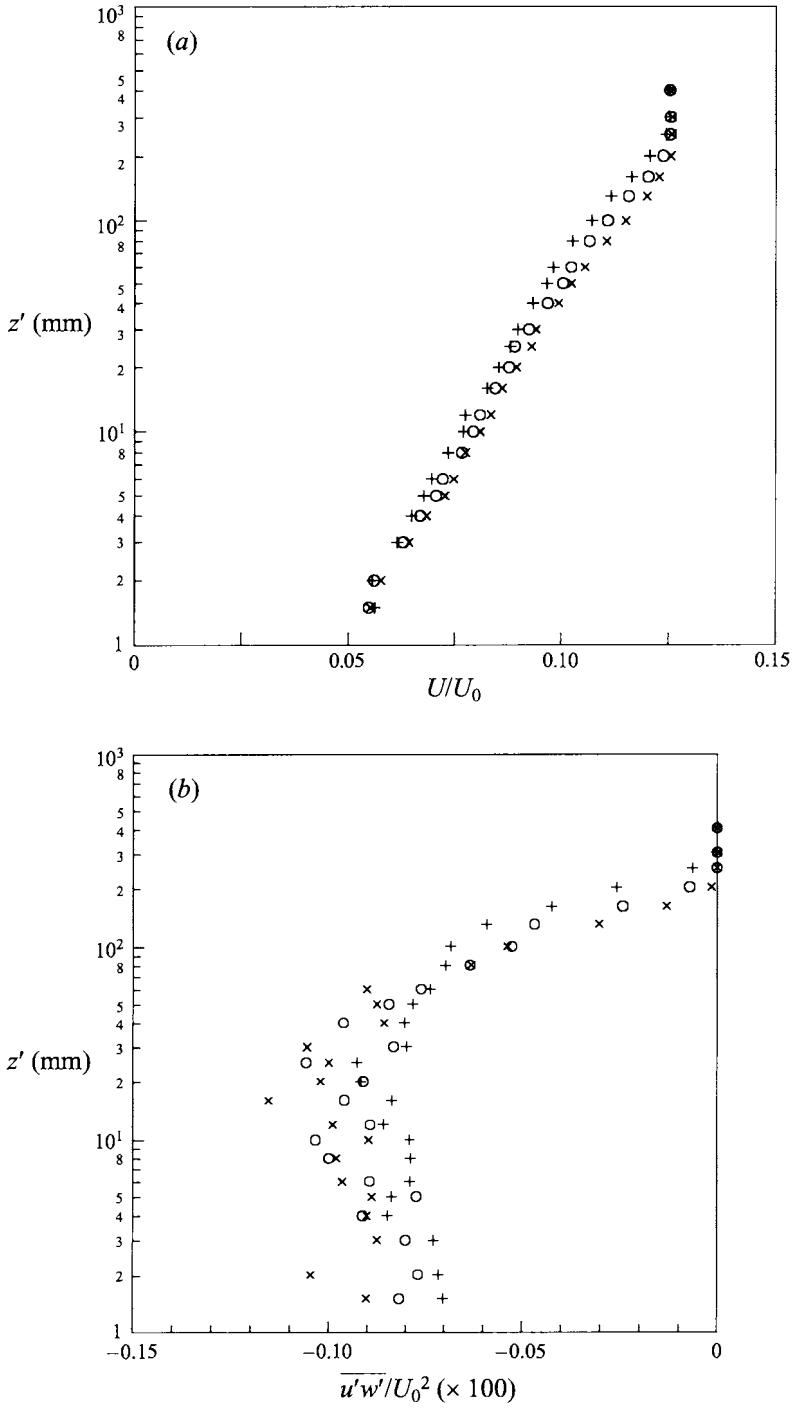

FIGURE 3(*a*, *b*). For caption see facing page.

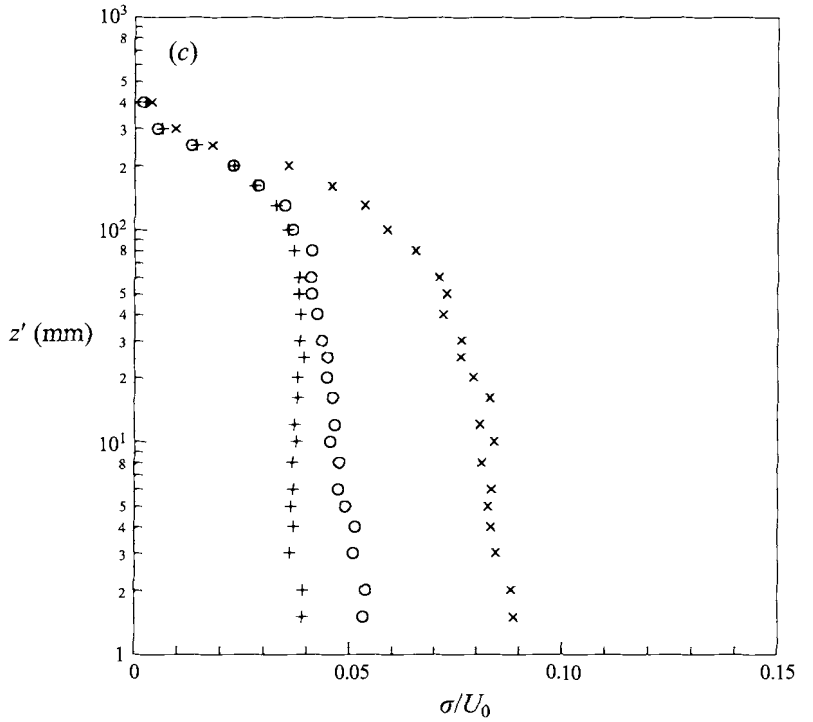

FIGURE 3. Flow measurements over the Masonite-covered flat floor of the wind-tunnel: (*a*) mean velocity at three locations, $x = 6.7$ m (×), 10.4 m (○) and 14.0 m (+) downstream from the honeycomb; (*b*) shear stress at the same three locations, (*c*) normal stress components at $x = 14.0$ m (×, σ_u; ○, σ_v; +, σ_w).

(0.085, 0.055, 0.035). Atmospheric boundary layers generally have slightly higher values of σ_v and σ_w as illustrated by the average flat-terrain σ/u_* values (2.39, 1.92, 1.25) given by Panofsky & Dutton (1983, p. 160). The near-surface values of $-\overline{u'w'}$ (0.0007 to $0.001U_0^2$) are however significantly lower than the corresponding u_*^2 values from the velocity profiles ($\sim 0.0017U_0^2$), although downward extrapolation of the measured $-\overline{u'w'}$ profiles (figure 3*b*) from $z' = 30$ mm to the surface would give values which were more or less consistent with the profile u_*^2. Our suspicion is that this is due to limitations of the X-wire measurement in the lowest 10–30 mm of the boundary layer, possibly associated with probe holder interference as well. Lawson & Britter (1983) discuss the yaw response of heated cylindrical sensors at low velocities and show that correction factors ranging from 1.2 to 2 (corresponding to a velocity range of 8 to 0.5 m s^{-1} in their experiment) should be applied to X-wire measurement of shear stress. Discrepancies in surface shear stress between X-wire measurements and the evaluation from the mean velocity profile can also be found in other wind tunnel simulations, e.g. Klebanoff (1955), Teunissen & Flay (1981).

Lateral uniformity of the flow over the flat floor was examined in the central third of the wind tunnel width at two heights, 20 and 100 mm, 14.0 m downstream from the honeycomb. The tests showed that the lateral variability was less than $\pm 2\%$ for the mean flow and $\pm 7\%$ for the turbulence components. These results confirmed earlier measurements by H. W. Teunissen (personal communication).

No measurements were made in the wind tunnel over the plane rough (carpet) surface. However, the measurements at a reference location about 2λ upstream of the waves are sufficient to describe the undisturbed flow in this case. The mean flow measurements give $z_0 = 0.4$ mm as noted above and, from the velocity profile, $u_* =$

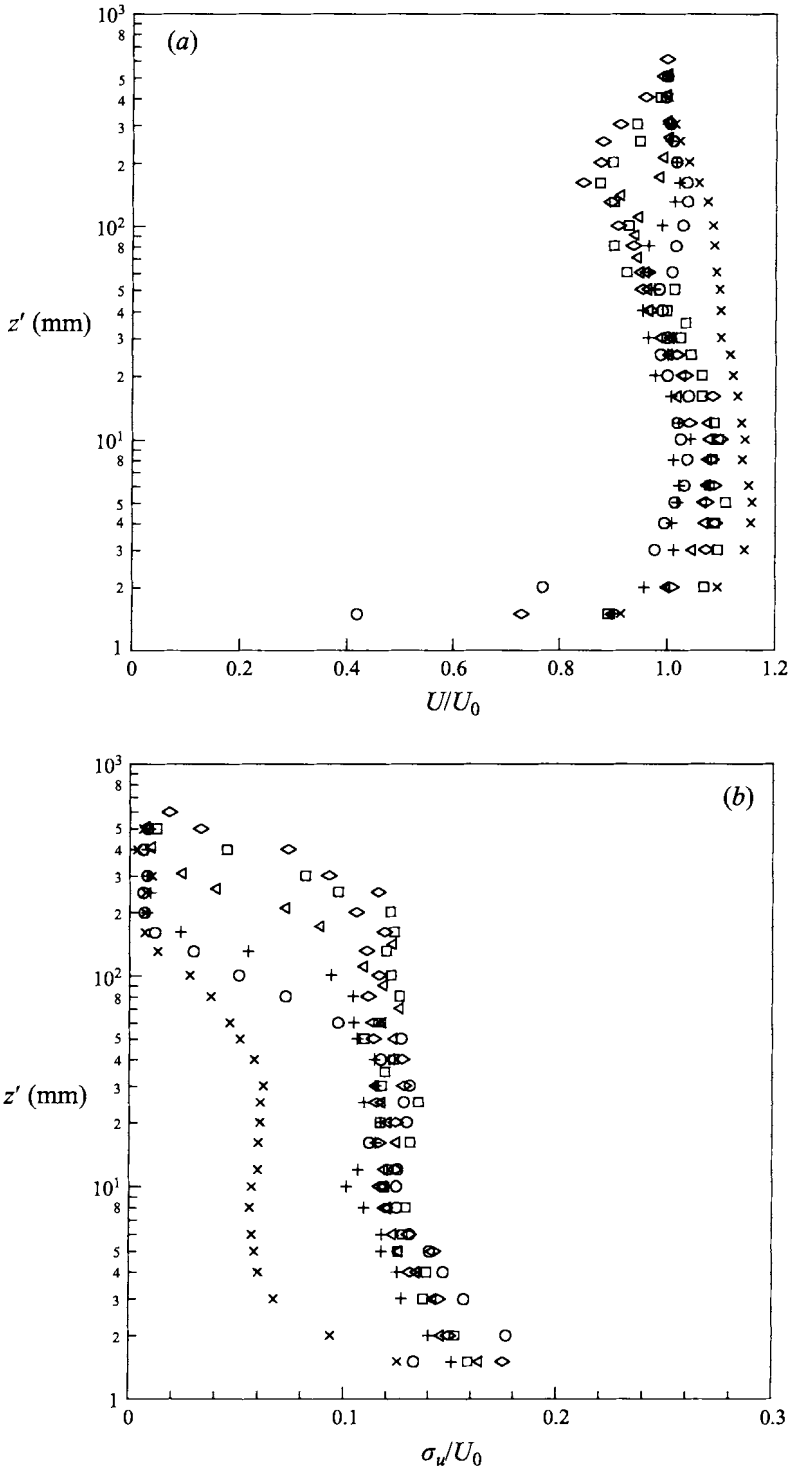

FIGURE 4. Flow measurements over the wave crests (smooth case) (*a*) U/U_0, (*b*) σ_u/U_0 (×, 1st crest; ○, 2nd crest; +, 3rd crest; ◁, 6th crest; □, 10th crest; ◇, 14th crest).

0.62 m s^{-1} with $U_0 = 10$ m s^{-1} at this location. With a roughness Reynolds number of about 16, the flow is aerodynamically rough. Values of $(\sigma_u, \sigma_v, \sigma_w)/u_*$ are (1.5, 1.0, 0.8), with $(\sigma_u, \sigma_v, \sigma_w)/U_0 = (0.096, 0.063, 0.047)$. Again, the near-surface X-wire measurement of $-\overline{u'w'}$ $(0.0015U_0^2)$ is lower than u_*^2 determined from the velocity profile $(0.0038U_0^2)$.

4. Measured flow structure over the waves in the central plane of the wind tunnel

The three-dimensional secondary flow features discovered in our flow over the relatively smooth-surfaced waves will be discussed below in §6. First we will discuss flow measurements made in the central plane of the wind tunnel ($y = 0$), ignoring the lateral variations and any secondary flow. Limited, single hot-wire profile measurements at locations away from the central plane (at $y = \pm 400$ mm for downstream locations between the 11th and 12th crests) showed along-wave (x) and vertical (z') structure of the topographically induced flow modification in U and σ_u similar to that observed along the centreline.

4.1. *Establishment of the periodic flow*

When boundary-layer flow encounters a train of waves, over the first wave it will respond more or less as in the case of a single hill, while over subsequent waves the flow could be quite different since the oncoming flow has been modified by the waves upstream. After some adjustment over the first few waves, we expect the lower part of the flow to approach a near-equilibrium, and approximately spatially periodic state, since the underlying topography is periodic. Counihan (1974) concluded, from his observations, that the flow becomes essentially periodic downstream of the third wave crest. We would, however, expect a general reduction in flow speed at upper levels within the boundary layer as the flow progresses downstream, due to boundary-layer growth, which will itself be enhanced by the drag increase caused by the topography.

Vertical profiles of the mean streamwise velocity and the turbulence component σ_u (defined in streamline coordinates) at wave crests for the smooth surface are given in figure 4. These were all measured in the central plane ($y = 0$) of the tunnel. The wind tunnel roof was readjusted after insertion of the model in the test section to maintain a zero longitudinal pressure gradient in the outer flow over most of the section of the tunnel containing the wave model and the free-stream velocity was maintained at approximately 10 m s^{-1}. The flow reaches an almost periodic state quite rapidly, after the third or fourth wave, especially at low levels. Mean velocities are seen to be significantly greater than the upstream flat-floor values (figure 3*a*) at low levels over all the crests, with maximum speed-up occurring over the first crest. Turbulence (σ_u) is found to decrease relative to the upstream flat-floor values in the accelerated flow over the first crest, as expected on the basis of rapid distortion theory (see Kaimal & Finnigan 1994, p. 183), but is stronger than upstream over subsequent crests as a result of a general increase in turbulence levels over the waves. As indicated by the σ_u profiles in figure 4(*b*), the boundary-layer depth has increased from about 200 mm upstream of the model to about 600 mm above the 10th to 15th crests. Most of the growth occurred over the first few waves.

4.2. *Mean velocity and surface pressure structure in well-established periodic flow*

Figure 5(*a*, *b*) shows vertical ($\log z'$) profiles of mean velocity at selected downstream locations between the 11th and 12th wave crests in the relatively smooth and rough

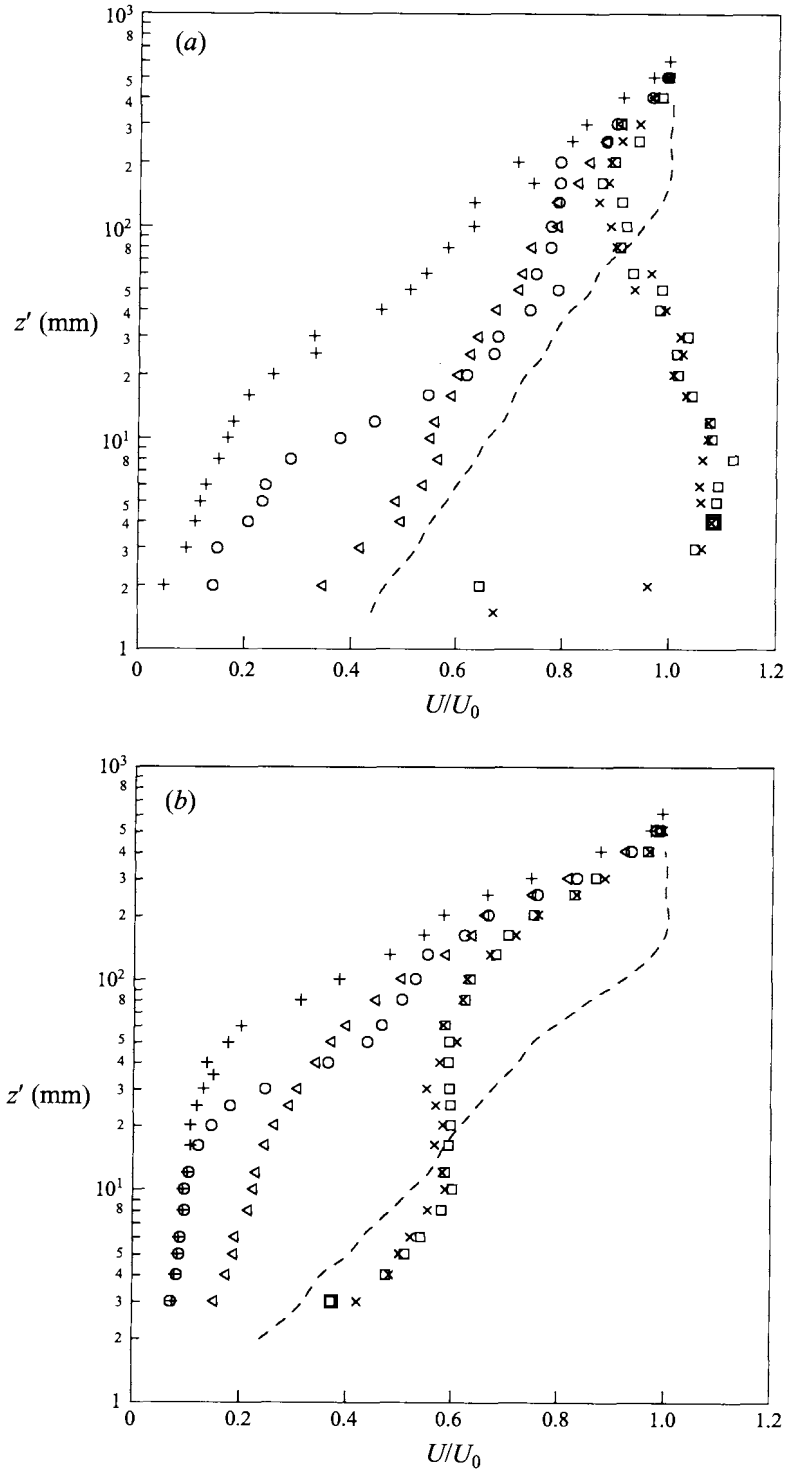

FIGURE 5(*a*, *b*). For caption see facing page.

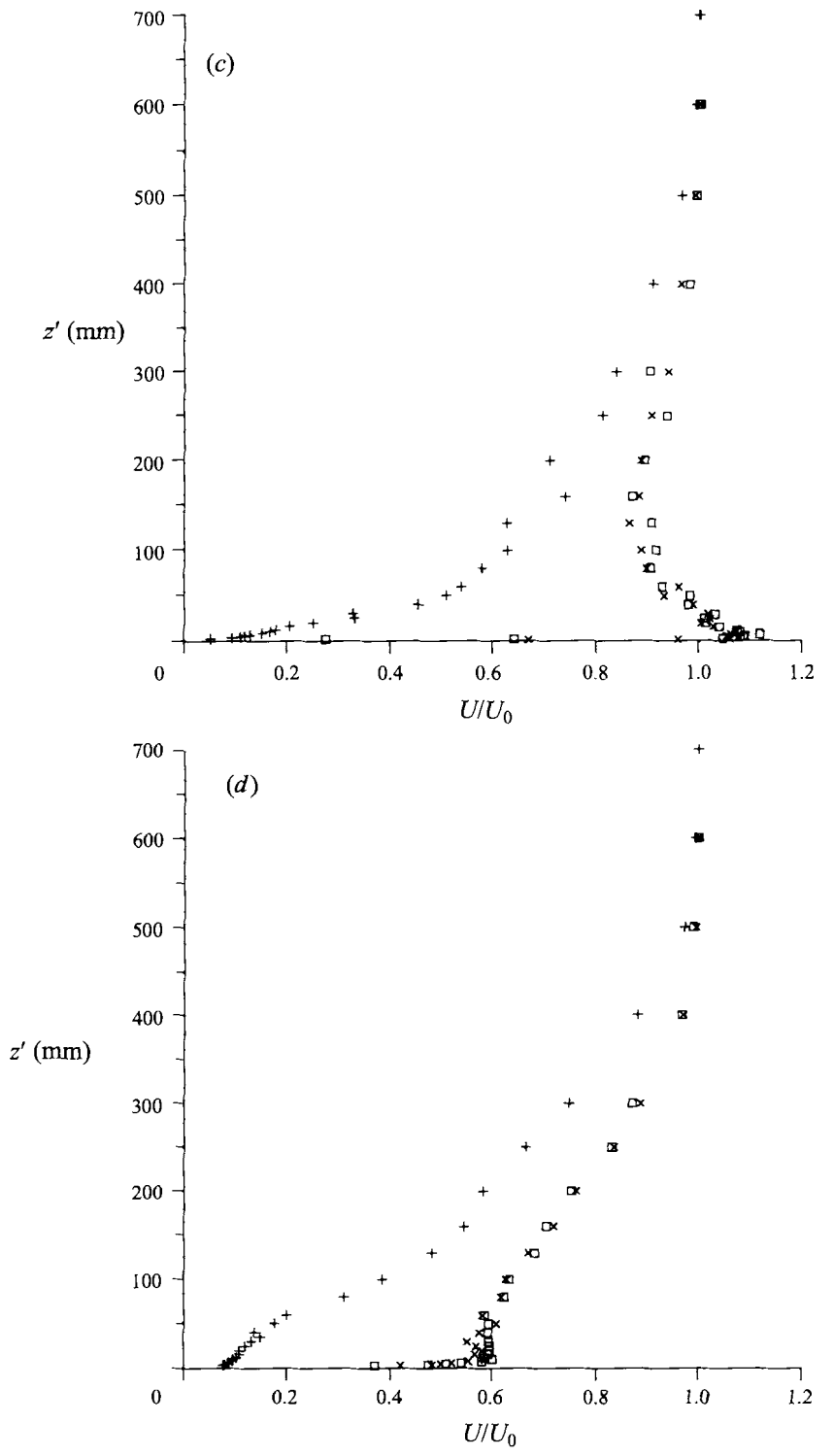

FIGURE 5. Mean velocity profiles: (*a*, *b*) U/U_0 *vs.* $\log z'$ at locations between the 11th and 12th wave crests over (*a*) relatively smooth-surfaced waves and (*b*) rough-surfaced waves. (*c*, *d*) U/U_0 *vs.* z' at crests and troughs over (*c*) relatively smooth-surfaced waves and (*d*) rough-surfaced waves. ——, Upstream reference profile (*a*, *b*); single-wire measurements (×, 11th crest; ○, midway down wave 11; +, 11th trough; ◁, midway up wave 12; □, 12th crest).

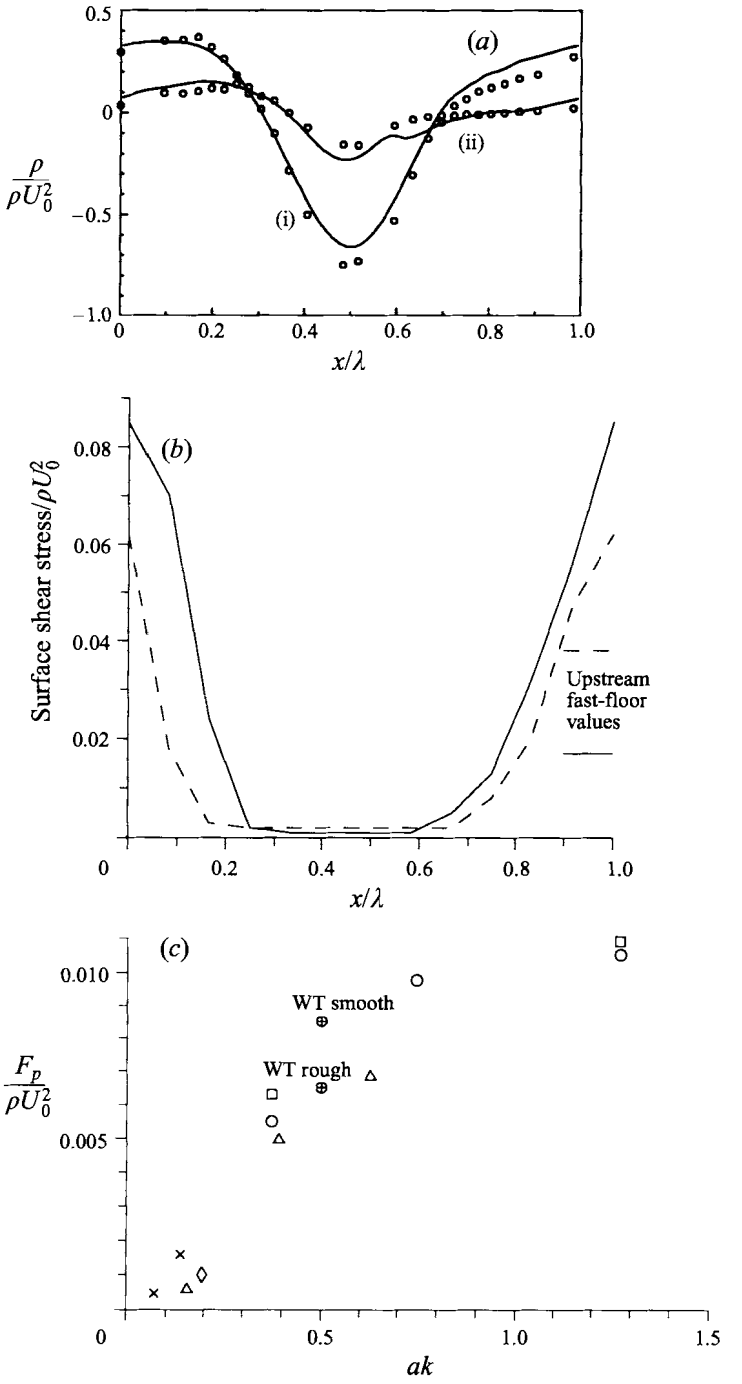

FIGURE 6. (*a*) Surface pressure ($p/\rho U_0^2$) over the 10th wave. ○, Measurements; and LES predictions: curve i, relatively smooth-surfaced waves ($z_0 = 0.03$ mm); curve ii, rough waves ($z_0 = 0.4$ mm). (*b*) Surface shear stresses, normalized by ρU_0^2, from the wind tunnel study between 11th and 12th crests, estimated from velocity measurements at $z' = 3$ mm and prescribed z_0 values: ——, relatively smooth-surfaced waves ($z_0 = 0.03$ mm); – – –, rough waves ($z_0 = 0.4$ mm). (*c*) Form drag for this and other laboratory studies of flow over wavy surfaces with various slopes (ak). ⊕, Present study, Beebe & Cermak (1972); □, $U_0 = 6$ m s^{-1}; ○, $U_0 = 12$ m s^{-1}; △, Zilker *et al.* (1977, 1979); ◇, Kendall (1970); ×, Hsu & Kennedy (1971).

Surface type	$(u_*^2)_0$	$\langle u_*^2 \rangle$	F_p	$\langle u_*^2 \rangle + F_0$	MTB
Rel. smooth	0.0017	0.0025	0.0085	0.0110	0.0092
Rel. rough	0.0038	0.0014	0.0065	0.0079	0.0127

TABLE 1. Drag values over the waves: wind tunnel study. All drag values are per unit area and are normalized by ρU_0^2; $(u_*^2)_0$ is upstream or flat-floor stress from the velocity profile, wavelength-averaged, $\langle u_*^2 \rangle$, values are calculated assuming local logarithmic profiles near the surface with the roughness lengths determined from the upstream or flat-floor measurements, F_p is normalized form drag, calculated from (4), MTB is total drag computed from the momentum budget over 10 waves

surface cases respectively. The profiles over the 11th and 12th crests match very well and there is also good agreement between repeated measurements of the same profiles with single-wire and cross-wire probes. Note that the flow over the waves is very sensitive to surface roughness. The increase in z_0, by an order of magnitude, between our smooth and rough cases, greatly reduces the speed-up over the crests and increases the velocity reduction in the outer part of the boundary layer, although the boundary-layer depth is hardly affected.

Flow separation was expected in the troughs since the maximum slope (ak) is 0.5 in the present case, and $ak \sim 0.3$ was considered to be the critical slope for separation (cf. Kuzan *et al.* 1989, figure 1). For both the relatively smooth and rough cases, flow in the first trough (not shown) was strongly separated, as indicated by both tuft tests (wool tufts attached at the surface) and surface pressure measurements. For the smooth waves, tuft tests showed occasional intermittent reverse or cross-stream flow over a limited section of the lee slope in the 10th trough but (see figure 6*a*) there was no constant-pressure region. Although intermittent separation probably occurs it is limited in extent and the mean flow remains essentially attached. No tuft tests were conducted over the rough waves but pressure measurements show regions of near-constant surface pressure on the downwind slope of the wave indicating separation, over both the first and the tenth troughs. As seen in figure 6(*a*), the constant (approximately) pressure region extends from $x/\lambda = 0.15$ to 0.5 in the 'rough' case while surface pressures increase continuously between crest and trough in the 'smooth' case. Our hot-wire instruments could not differentiate between positive and negative velocities and are unreliable in regions of high turbulence intensity. However our subjective interpretation of the velocity profiles in figure 5 is that there is little or no reverse flow in the 'smooth' wave case while in the rough case the flow may have a separated, essentially stagnant, wake region extending to heights of order 20 mm (0.4*a*) on the lee slope and in the trough.

Figures 5(*c*) and 5(*d*) show the same velocity profiles as figures 5(*a*) and 5(*b*) but with a linear z' scale rather than a logarithmic one. We do this to clearly illustrate the strong relatively shallow jet above the crests in the flow over the 'smooth'-surfaced waves (figure 5*c*). Frictional effects only seem to affect the flow at the very lowest levels. Linear inviscid irrotational flow over small-amplitude sinusoidal waves would have the velocity perturbation or speed-up decaying with height as $\exp(-kz)$ – see for example Walmsley, Salmon & Taylor (1982). The observed decrease in speed above the near-surface jet shown in figure 5(*c*) appears to approximately match this but we have so far been unable to simulate such large velocities and shallow jets with models based on the Reynolds-averaged equations (see Taylor *et al.* 1995). In the rough-wall case the near-surface flow above the crests has substantially lower velocity than the smooth case and the pronounced near-surface jet is absent. Figures 5(*c*) and 5(*d*) can be compared to

the results presented for aerodynamically smooth wavy surfaces by Counihan (1974), Buckles *et al.* (1984) and Kuzan *et al.* (1989). Buckles *et al.* measured velocity profiles above aerodynamically smooth waves with maximum slope $ak = 0.628$, for which the flow was strongly separated. Their crest and trough profiles (see figures 8 and 9 of their paper) are in reasonable qualitative agreement with our separated-flow case (figure 5*d*) showing very strong shear close to the surface above the crest, with nearly constant velocity above that up to $z'/\lambda \approx 0.1$ and then a gradual increase with z' to free-stream or channel maximum velocity. Kuzan *et al.*'s experiment 1 (see their figure 3) with $ak = 0.393$ has 'incipient' or transitional separation and might be expected to be qualitatively similar to our relatively smooth-wall case (figure 5*c*). Their trough profile shows a similar pattern with moderate shear from the surface up to $z' \approx 0.1\lambda$ and weak shear above that. Their crest profile has strong shear close to the surface but then approaches the free-shear value monotonically. Counihan's (1974) configuration A and D cases have $ak = 0.52$, very close to ours, and the flow appears to remain attached after the second crest. Neither Counihan's nor Kuzan *et al.*'s crest profiles display the jet feature that we observed. The same is true of results presented by Bandou & Mitsuyashi (1988) for flow over waves with $ak = 0.314$. However, Motzfeld's (1937, figure 10) profiles for the flow over his second-wave model ($ak = 0.314$) do show a near-surface jet above the wave crest, although it is less pronounced than ours.

Returning to the pressure measurements (figure 6*a*) we note first that the range of the pressure perturbation measured in the essentially attached flow over the relatively smooth surface ($0.57\rho U_0^2$) is roughly four times that measured for the flow over the rough waves ($0.15\rho U_0^2$). This is approximately consistent, through the Bernoulli equation for inviscid flow ($p+\frac{1}{2}\rho U^2 = \text{constant}$), with near-surface crest-to-trough velocity squared differences computed from the profiles shown in figure 5 (approximately $1.2U_0$ for the smooth case and $0.35U_0$ for the rough case). The lower perturbation pressure ranges in the rough-wall case are presumably due to the smoothing of upper flow streamlines, relative to the topography, as a result of flow separation. Note that the range of pressure variation along the relatively smooth-surfaced wave ($1.14ak\rho U_0^2$) is significantly lower than the predictions of linear inviscid irrotational flow theory ($2.0ak\rho U_0^2$) as a result of both velocity shear and nonlinear effects. Surface pressure distributions are qualitatively similar to those observed over aerodynamically smooth waves by Kuzan *et al.* (1989) where varying slope and Reynolds number determine whether or not the flow will separate. Some of their results (their figure 22) with $2a/\lambda = 0.125$ ($ak = 0.393$) show steady shallow separated flow at a Reynolds number Re (based on bulk velocity, U_b, and channel half-height) of 13200 while at high Re (48000) there is only intermittent separation. The corresponding ranges of pressure variation are approximately $0.7ak\rho U_b^2$ and $1.65ak\rho U_b^2$, where U_b may be slightly (5%) lower than U_0. For steeper waves ($2a/\lambda = 0.2, ak = 0.628$) the normalized pressures are reduced.

The pressure range over our rough-surfaced waves is approximately $0.3ak\rho U_0^2$. The separated aerodynamically smooth channel flow over wavy surfaces reported by Buckles *et al.* had a surface pressure range of about $0.2\rho U_b^2$ or $0.33ak\rho U_b^2$, in good agreement assuming $U_b \approx U_0$. The overall shape of the distribution was also similar to ours but with a rather sharper pressure minimum over the crest. The same is true of the early measurements by Stanton *et al.* (1932) for waves with $ak = 0.64$. Pressure ranges on their 10th and 27th waves varied significantly with Reynolds number, but $0.2\rho U_0^2 = 0.31ak\rho U_0^2$ is a representative value.

4.3. *Surface drag and the momentum budget*

From our surface pressure measurements (which were to within 2% of the pressure-range over the waves in repeated tests) we computed the form drag per unit area on the waves, i.e.

$$FD = \rho U_0^2 F_p = \int p_s^* (\mathrm{d}z_s/\mathrm{d}x)\,\mathrm{d}x/\lambda, \tag{4}$$

where p_s^* is the surface normal stress, $p+\overline{u_n'^2}$, and the integral is over one wavelength. The results are given in table 1, together with estimates of the wavelength-averaged surface shear stress and the total horizontal stress on the lower boundary based on momentum budget calculations. Upstream surface shear stresses, estimated from profile $u_*^2 s$ as discussed in §3, are also given.

We were unable to directly measure the shear stress on, or sufficiently close to, the wavy surface (see discussion of the stress gradients below). Although assumptions of local equilibrium flow with logarithmic velocity profiles close to the surface are clearly somewhat suspect, we have considered it worthwhile to compute surface friction velocities based on our velocity measurements at $z' = 3$ mm for twelve equally spaced locations along the waves. In effect we use a drag coefficient for a height of 3 mm, derived for equilibrium flow over a flat surface, to provide an estimate of the surface stress over the curved surface of the wave model. The rationale for this is that the velocity measurement height, 3 mm, is much less than the radius of curvature of the surface (200 mm) so that curvature effects will be negligible and the surface could be considered as flat, and within the Jackson–Hunt (1975) inner layer of depth l and thus at a height where the velocity will be affected by the topographically modified shear stress. Values of l for the relatively smooth- and rough-surfaced waves are 8.5 mm and 13.6 mm respectively. The calculated shear stresses are plotted in figure 6(*b*) and are used to obtain wavelength-averaged surface shear stress estimates. There is clearly some uncertainty about the accuracy of this approach, and even about the direction of the shear stress in the separated region, but we would argue that they do provide useful estimates. Note that the surface friction velocities in the separated region are relatively low and, when integrated over a wavelength for the rough-surface case, only 7% of the total shear stress comes from the 50% of the surface ($0.2 < x/\lambda < 0.7$) where separation is most likely.

Momentum budget calculations were attempted for control volumes over a single wavelength ($0 < x/\lambda < 1$ in figure 1) from the surface to the top of the boundary layer ($z_s \leqslant z \leqslant \lambda$) and also from the surface to $z = a$ (requiring an integral of $UW+\overline{u'w'}$ at $z = a$). However, the net drag was a small residual and could not be reliably determined. We had more success with a momentum budget for a control volume extending over ten wavelengths (crests 4–14). There is an assumption of two-dimensionality built in to the budget and even over ten wavelengths we are still seeking a residual which is of order 10% of the total momentum flux ($\sim \rho U_0^2 \lambda$, since we integrated up to a height equal to the wavelength).

The budget for the smooth case looks satisfactory (only 16% discrepancy between the total drag and the momentum budget estimate), considering the assumptions involved. The form drag is more than three times the wavelength-averaged surface shear stress and this average surface shear stress is a little higher than the flat-floor value. In the rough-surface case there is a significant imbalance in the budget and we are uncertain where the error has occurred. The sum of form drag plus surface shear stress indicates a total which is roughly double the upstream flat-floor value although

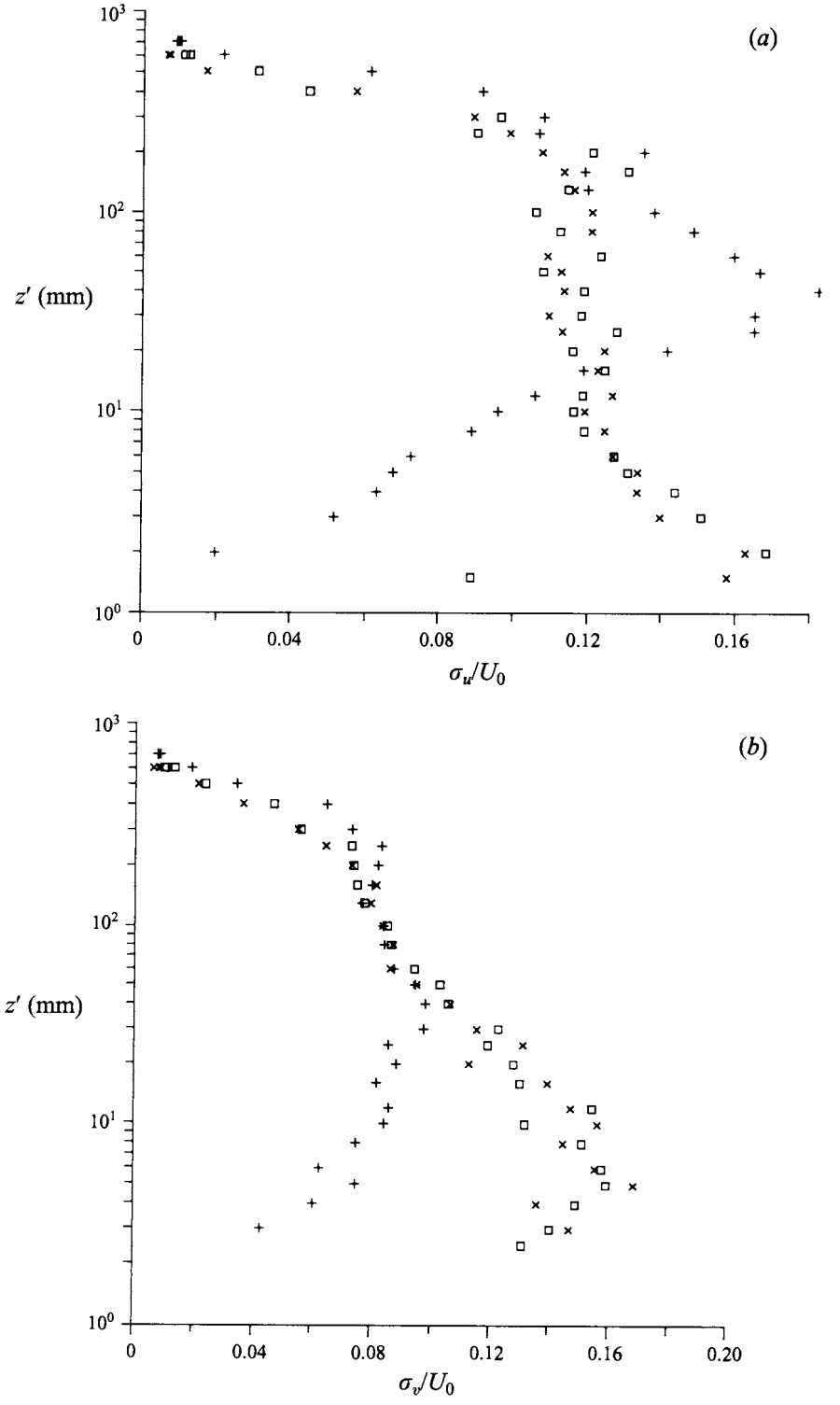

FIGURE 7(*a*, *b*). For caption see facing page.

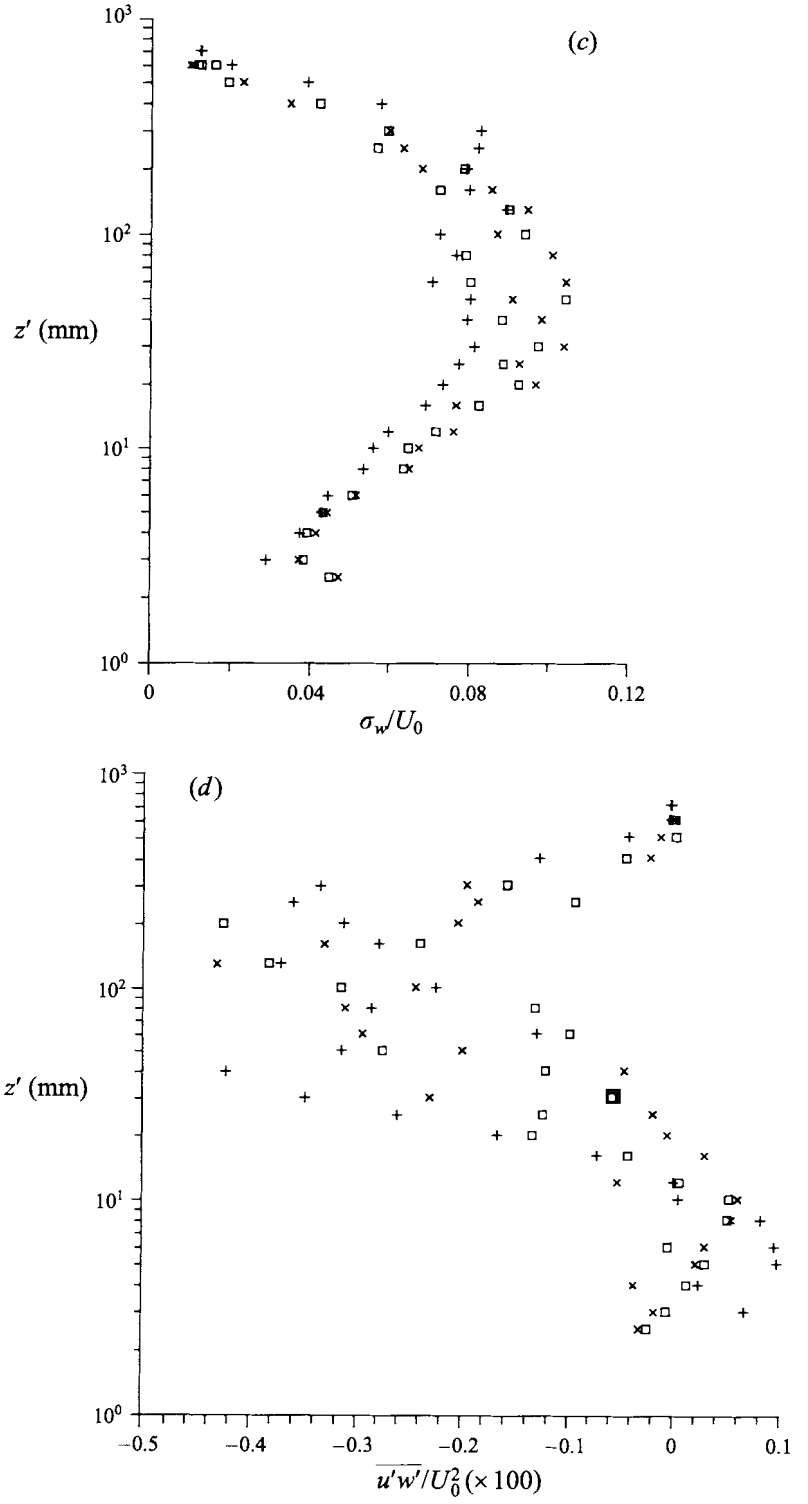

FIGURE 7. Profiles of (*a*) σ_u/U_0, (*b*) σ_v/U_0, (*c*) σ_w/U_0 and (*d*) $\overline{u'w'}/U_0^2$ above crests 11 and 12 and the intervening (11th) trough for flow over the relatively smooth-surfaced waves: ×, 11th crest; +, 11th trough; □, 12th crest.

the estimated wavelength-averaged surface shear stress is only 37% of the upstream value. Near the crests the local shear stress is high ($0.0062\rho U_0^2$), as seen from figure 6(*b*), but not as high as in the smooth case ($0.0085\rho U_0^2$). The shear stress is negligible over half the wavelength and only exceeds the upstream value over about one sixth of the wave. The form drag is less than that measured over the relatively smooth waves.

The form drag measurements are compared to results from other laboratory studies, all over aerodynamically smooth surfaces, in figure 6(*c*), showing form drag variation with slope (*ak*). Although there is considerable scatter there is consistency with the other studies. For low values of *ak*, we expect from linear theory that $F_p \propto (ak)^2$. This rate of increase is unlikely to be maintained for large *ak*. In fact, as indicated from figure 6(*c*), the form drag seems to level off as *ak* increases beyond 1.0.

Estimates of the wavelength-averaged turbulent shear stress, $\langle -\overline{u_n' u_s'} \rangle$, at $z' =$ 200 mm ($\lambda/3$), based on measurements at 13 points along the wave, are $0.0035U_0^2$ and $0.0038U_0^2$ for the smooth and rough cases respectively. These are larger than the estimated surface shear stresses but lower than the total horizontal stresses on the surface, in accord with the model proposed by Taylor *et al.* (1989).

4.4. *Centreline turbulence statistics*

Turbulence data were obtained with single wires and with X-wires oriented both vertically (X, Z) and horizontally (X, Y). All of the measurements generated data on σ_u while the X-wire measurements generated profiles of σ_v, σ_w, $\overline{u'v'}$ and $\overline{u'w'}$. All of the turbulence measurements are presented in streamline coordinates (i.e. $u' = u_s', v' = v'$, $w' = u_n'$). Data are available at various locations between the 11th and 12th wave crests but we will focus on crest and trough profiles.

Figure 7(*a–d*) and 8(*a–d*) show profiles of $\sigma_u, \sigma_v, \sigma_w$ and $\overline{u'w'}$ above crests 11 and 12 and the intervening (11th) trough for the relatively smooth- and rough-surface flows respectively. They warrant careful examination. First we see that the total boundary-layer depth at these locations is of order 600 mm in both the rough and smooth cases, roughly double the depth in the smooth-surface flat-floor case (figure 3). However, above $z' = 300$ mm turbulence decreases with height and modifications to turbulence in the outer half of the boundary layer may be somewhat different than those determined by models based on perturbations from constant-stress-layer flow. As noted earlier, inner-layer depths obtained using the Jackson–Hunt equation are 8.5 mm and 13.6 mm for the smooth and rough cases respectively. Since these are substantially less than 300 mm we can reasonably expect that the dynamics of the mean flow perturbations will not be significantly affected by the limited depth of the boundary layer.

Turbulence levels (σ/U_0 values) are generally higher than the upstream or flat-floor values presented in §3. In the relatively smooth-wall case, at heights (z') of order 100 mm, crest and trough values are essentially equal and increases relative to flat-floor values are about 25% for σ_u, 45% for σ_v and 100% for σ_w. Corresponding values in the rough case, relative to upstream, are 35%, 45% and 60%. With or without flow separation the waves produce a more turbulent flow. The σ_u data show good consistency between all three measurement systems above the crests but in the trough, data obtained with the X-wire oriented in the (X, Z)-plane were somewhat different below $z = 20$ mm from those with the U-wire and X-wire in the (X, Y)-plane. Mean flow velocities are low in this region leading to high turbulence intensities ($\sigma_u/U_0 =$ 50%) and all measurements will be somewhat unreliable. Only U-wire data are plotted in figures 7(*a*) and 8(*a*).

4.4.1. *Relatively smooth-wall data*

Near the surface ($z < 10$ mm) we find lower σ_u and σ_v values (figure 7*a*, *b*) over the trough than over the crest as might be expected if this near-surface layer were tending towards local equilibrium. The near-surface σ_w profiles (figure 7*c*) indicate similar values over the crest and trough although there is a hint from the lowest measurement levels that values may increase close to the surface above the crest. At heights of order 20 mm and above, higher σ_u and lower σ_w values over the trough compared to the crest are qualitatively consistent with rapid distortion theory (RDT, see for example Britter, Hunt & Richards 1981 or Newley 1985) and with the predictions made by Ayotte *et al.* (1994) for small-amplitude waves. For plane strain of initially axisymmetric ($\sigma_v = \sigma_w$) or isotropic turbulence ($\sigma_u = \sigma_v = \sigma_w$), in the flow over an isolated two-dimensional ridge, Newley predicts, to first order, that

$$(\Delta\sigma_u^2/\sigma_u^2)/(\Delta U/U) = -0.8,$$

where Δ can indicate trough to crest differences. In our case, at $z' = 40$ mm, the height of the maximum difference in σ_u, we estimate $\Delta\sigma_u^2/\sigma_u^2 \approx -0.7$ and $\Delta U/U \approx 0.7$. The ratio, -1.0, is in good agreement considering the large amplitude of the differences. Corresponding RDT results for σ_v and σ_w, assuming initially axisymmetric turbulence, are

$$(\Delta\sigma_v^2/\sigma_v^2)/(\Delta U/U) = -0.8(R-1.0) \approx -0.8$$

and

$$(\Delta\sigma_w^2/\sigma_w^2)/(\Delta U/U) = (1.2-0.4R) \approx 0.4,$$

where the anisotropy ratio, $R = \sigma_u^2/\sigma_w^2 \approx 2.0$ in our case. The measured σ_w data near $z' = 40$ mm are rather scattered but on average give a value of approximately $+0.44$ for the trough to crest difference ratio, in general agreement with the RDT estimate. The σ_v plot (figure 7*b*) indicates that the difference ratio is reducing with height from about $+1.3$ at $z' = 10$ mm to 0 at $z' = 60$ mm. It appears to be positive to all heights in contrast to the RDT estimate. Large discrepancies between measurements and the RDT estimates (assuming axisymmetric turbulence) for σ_v were also noted by Gong & Ibbetson (1989) in a case of flow over a single hill.

At heights (z') about 200 mm the values of σ_u are slightly higher above the troughs than the crests. This also occurs for σ_v, σ_w and $-\overline{u'w'}$ and will be primarily due to the fact that a given value of z' will correspond to a higher value of z over the crest than the trough (by 96.5 mm). Streamlines are approximately horizontal above 200 mm and σ values are decreasing with z. Thus, even though σ values could be constant along a streamline, differences between crest and trough can appear when the profiles are plotted as functions of z'.

The general shapes of our σ_u profiles are quite similar to those presented (with a linear z' scale) by Kuzan *et al.* (1989, figures 3 and 4) although the values of σ_u/U_0 are lower by about 30%. The trough maximum of σ_u occurs at about $z' = 0.06\lambda$ in both cases (40 mm in our experiment). At the intermediate downslope location ($x = 0.25\lambda$) the σ_u profile is similar in shape to that shown for the trough but with the maximum value of 0.22 occurring lower at about $z' = 12$ mm. These maxima correspond to regions of increased velocity shear ($\partial U/\partial \ln z = z\,\partial u/\partial z$, see figure 5*a*), suggesting that increased shear production, as well as rapid distortion, may contribute to the higher σ_u levels.

Our profiles of σ_v (figure 7*b*) show high values over the crests and lower values above trough locations for $0 < z' < 40$ mm while crest and trough profiles of σ_w (figure 7*c*)

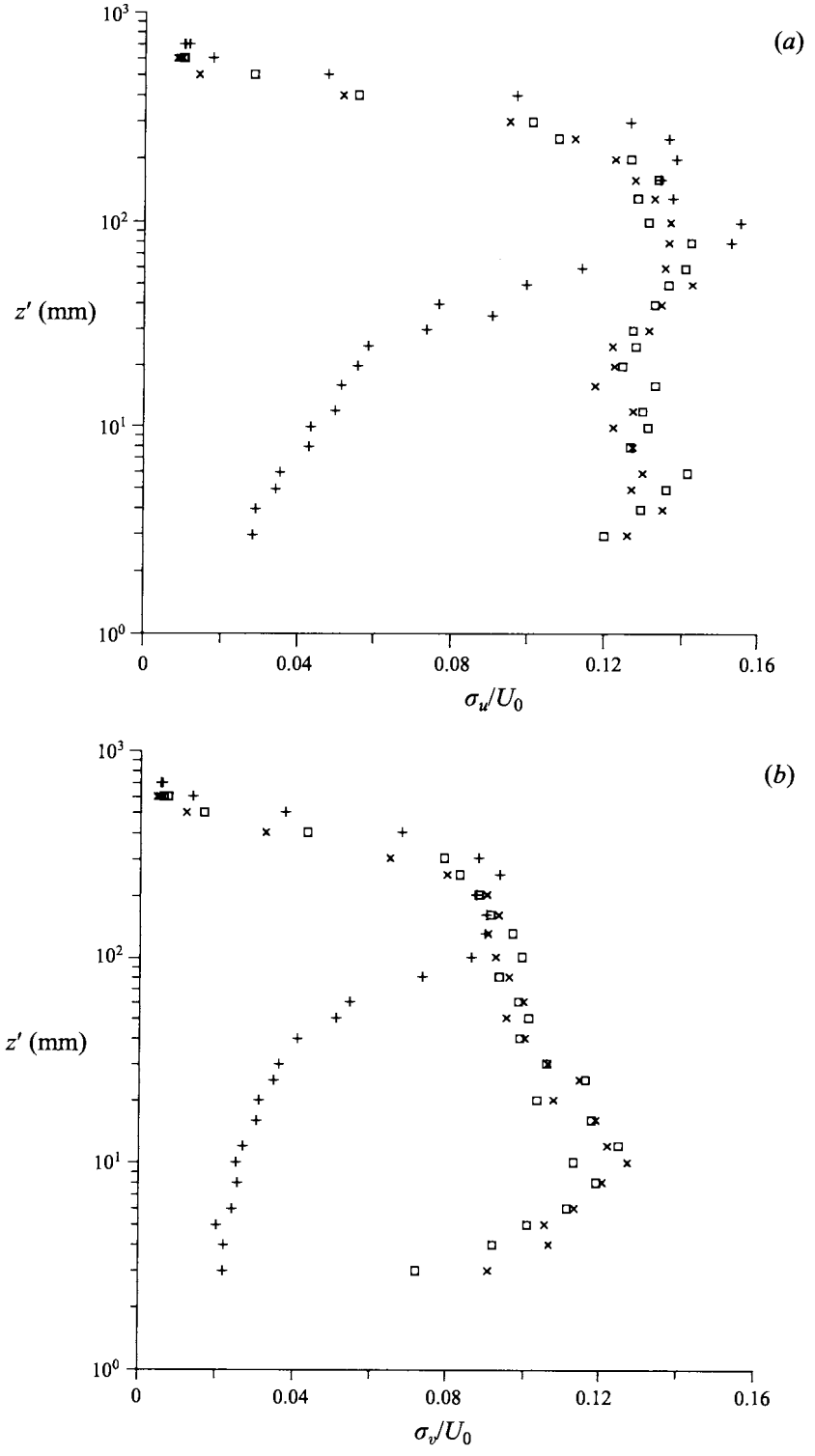

FIGURE 8(*a*, *b*). For caption see facing page.

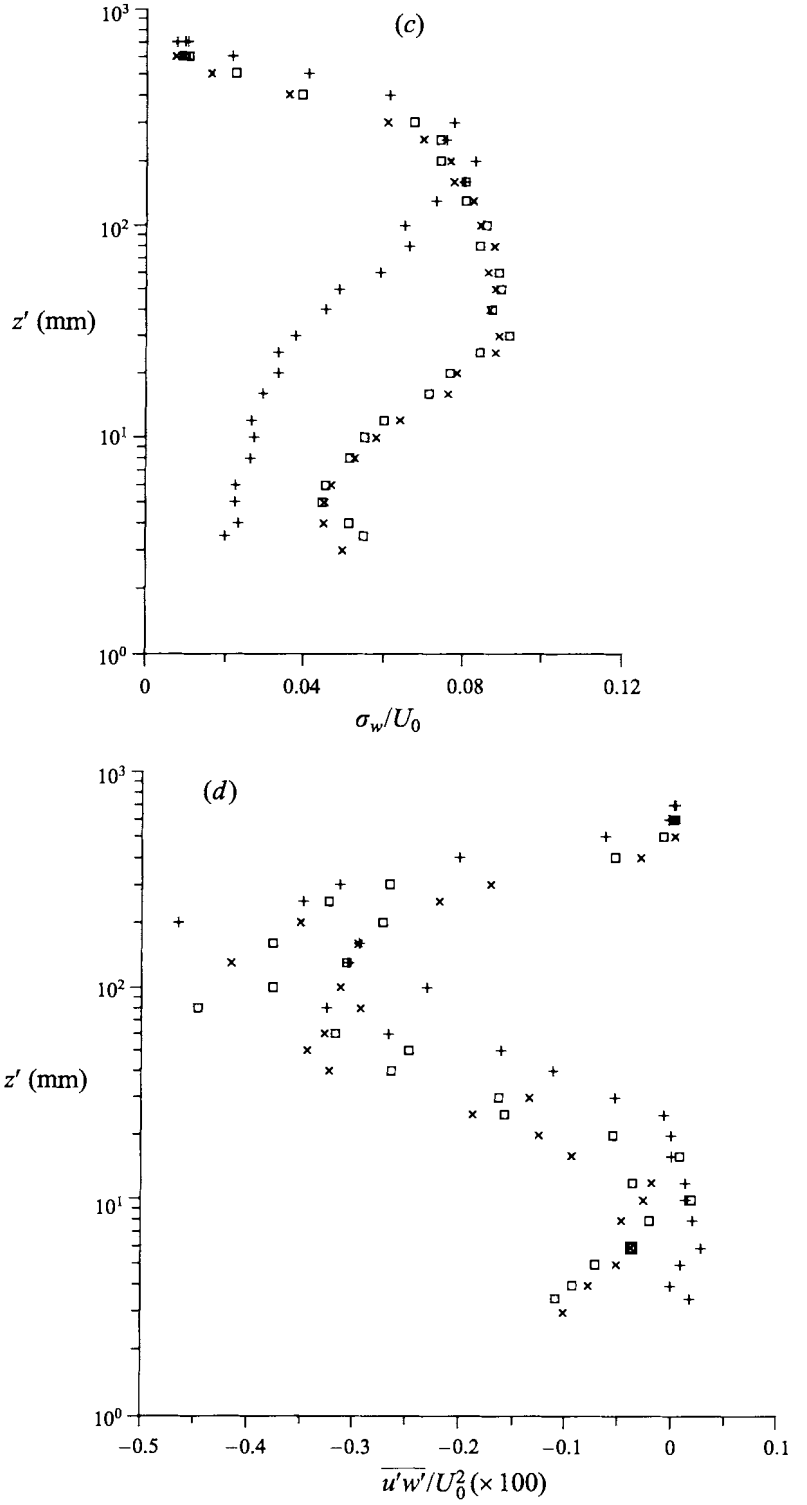

FIGURE 8. Same as figure 7 but for the rough-wave case.

are rather similar. Both have σ_w increasing with z' through the inner layer. Plots at the intermediate locations show the same behaviour. We can note that, at low levels, the ratio σ_w/σ_u is about 0.6 above the trough while it reduces to around 0.3 above the crest. The flat-floor boundary-layer value was 0.45, and was in agreement with other studies.

Streamline curvature effects (cf. Finnigan 1988; Finnigan *et al.* 1990; Ayotte *et al.* 1994) could be expected to cause σ_w increases in the trough and decreases over the crest, but there is no evidence of this in our data. At heights z' from 40 to 100 mm the σ_w maxima in the crest and trough profiles could be associated with secondary flows or large eddies, generated by the topography, filling the boundary layer and having high vertical velocities at mid-levels. Convective boundary layers (cf. Stull 1988, p. 125) generally show this behaviour. There is considerable scatter in our smooth-wall σ_w data, both between adjacent measurement levels in an individual profile and between the two crest profiles, in the $20 < z' < 200$ mm height range. This was not evident in the rough-wall case (figure 8*c*) and may be linked to large eddies or to unsteadiness of a secondary flow present in the smooth-wall case (to be discussed below), which could lead to slow temporal variations and inconsistencies between measurements at different levels since they were made at different times.

Turning to the $\overline{u'w'}$ data (figure 7*d*) we might first comment that there is considerable scatter between levels in the measured profiles, probably due in part to large-eddy or secondary flow effects, as for σ_w, and a possible need for longer averaging times in order to obtain completely stable statistics. However, we can see near-zero or positive values of $\overline{u'w'}$ for $z' \approx 10$ mm with a significant increase in shear stress ($-\overline{u'w'}$) with height above that over both crest and trough with values for $-\overline{u'w'}/U_0^2$ of order 0.003 at $z' = 100$ mm. These stresses are significantly larger than the flat-floor measurements (figure 3*b*, 0.001) and larger than the flat-floor log-linear profile estimates of u_*^2/U_0^2 (0.002, see §3 above). Thus the shear stresses in the outer part of the boundary layer are significantly increased by the presence of this wavy topography, which is consistent with the increased growth rate for the boundary layer. A rough estimate of $\partial(-\overline{u'w'})/\partial z$ in the outer layer gives $-0.004U_0^2$ over 200 mm ($\lambda/3$) which implies a deceleration rate of about 1.2% per wavelength at these levels from the balance between the horizontal advection and the vertical flux gradient. This matches well with the observed crest to crest velocity profile reductions shown in figure 4 indicating a velocity reduction of order $0.16U_0$ over 13 wavelengths. Low near-surface Reynolds stresses and large increases relative to upstream at heights of order $\lambda/6$ were also observed over wave crests by Counihan (1974) for his configurations (A and D) with $ak = 0.52$.

Despite the scatter and the possibility of measurement errors as we approach the surface it is apparent that the shear stress, above both crest and trough, is low for heights between 3 and 20 mm. Over the trough this is consistent with the low mean velocities found there. At mid-slope locations near-surface shear stresses are higher and the down-slope profile (for $x/\lambda = 0.25$, not shown) has a high-stress region ($-\overline{u'w'}/U_0^2 \approx 0.004$) near $z' = 10$ mm, corresponding (see figure 5*a*) to the high-shear location. As noted in Taylor *et al.* (1989, figure 1) the fact that the wavelength-averaged $-\overline{u'w'}$ generally increases with height in the lower part of this boundary layer over a wavy surface is linked to the fact that, in addition to the turbulent Reynolds stress, $-\overline{u'w'}$, there will also (in a Cartesian reference frame) be a non-zero wavelength-averaged mean flow Reynolds stress, $\langle -UW \rangle$. It is, however, still surprising that the near-surface stresses are so low over the crest. The assumption of local equilibrium near the surface would lead us to expect high values of $-\overline{u'w'}/U_0^2$ (≈ 0.0085) as

we approach $z' = 0$. However, the problems with measuring the Reynolds stress very close to the surface in either wind tunnel or field studies (e.g. Mickle *et al.* 1988) makes definitive observation difficult. Kuzan *et al.*'s (1989) measurements did not include $-\overline{u'w'}$ profiles but they do report surface shear stresses by Zilker which indicate maxima, a little upwind of the crest, of order $0.004U_0^2$, compatible with our estimates, given the different type of surface and different slope.

We need to explain how, above the crest, the shear stress goes from a supposedly high surface value to near zero between the surface and 3 mm. If we consider the U momentum equation in streamline coordinates, following Finnigan *et al.* (1990),

$$U\partial_x U = -(1/\rho)\partial_x p - \partial_x \overline{u'^2} + (\overline{u'^2} - \overline{w'^2})/L_a - \partial_z \overline{u'w'} + 2\overline{u'w'}/R,$$

where ∂_x and ∂_z are derivatives along and perpendicular to the streamlines and R and L_a are the local radii of curvature of the streamlines and a set of lines orthogonal to the streamlines, we find that the only terms large enough to balance the anticipated stress gradient ($\partial(\overline{u'w'})/\partial z \sim 0.0028U_0^2\,\mathrm{mm}^{-1}$) are the acceleration and pressure gradient terms. A possible magnitude for $U\partial U/\partial x$ (with the velocity going from near zero to $1.1U_0$ over a distance of 0.5λ at $z' \approx 3$ mm would be $0.004U_0^2\,\mathrm{mm}^{-1}$. We obtain a similar magnitude for $\partial p/\partial x$ on either side of the crest from figure 6(*a*). These terms would normally be in approximate balance but the acceleration term will formally be zero at the surface and, for these steep waves, the stress gradient needed to match a high local equilibrium value at the surface to the observed values at 3 mm and above does seem possible.

Relatively rough-wall data

In the rough-surface case the σ profiles above the trough (figure 8*a–c*) all show reduced values below about $z' = 50$ mm, corresponding, we assume, to the separation zone and relatively stagnant flow. The $\overline{u'w'}$ values in this region (figure 8*d*) are also near zero. Similar reductions in σ_u near the surface above the trough were observed by Buckles *et al.* (1984) in separated flow over steeper waves with an aerodynamically smooth surface.

The profiles show slightly higher σ_u and lower σ_w values above the trough than the crests near $z' \approx 100$ mm as in the smooth-wall case and as expected from rapid distortion calculations, noting that $\Delta U/U$ is smaller in this case. The σ_w profiles (figure 8*c*) have much less scatter than for the smooth-wall case. Above the inner layer, for $40 < z < 200$ mm, we again find increases in σ_w compared to the upstream value ($0.047U_0$) above crest, trough and (not shown) at intermediate locations, although peak σ_w values are less than in the smooth-wall case. We again associate these mid-level maxima with large eddies forced by the topography.

The rough-wall $\overline{u'w'}$ profiles are quite similar to those discussed above for the relatively smooth-surfaced waves although the lowest level $-\overline{u'w'}$ values above the crest (0.001 to 3 mm) do correspond to larger shear stresses. The crest value of u_*^2, based on an equilibrium-flow drag coefficient for $z' = 3$ mm, is however $0.0062U_0^2$, again indicating a significant near-surface shear stress gradient. Shear stress ($-\overline{u'w'}$) minima occur at heights (z') of order 10 mm while maxima, at $z' \approx 100$ mm, lie in the region of moderately high velocity shear (see figure 5*d*) and high turbulence levels (figure 8*a–c*).

The centreline mean flow and turbulence data presented above provide a basic picture of the flow above our wavy surfaces. There are clear qualitative differences between the relatively smooth- and relatively rough-surfaced flows. The flow clearly

separates over the rough-surfaced waves but not over the smooth. There is however an additional complication in the case of the relatively smooth-surfaced waves in the form of lateral (cross-flow) inhomogeneity. This is discussed in §6 below.

5. LES model results

Large-eddy simulations were conducted with a modified version of the model described by Dörnbrack & Schumann (1993) and based on the work of Krettenauer & Schumann (1992). The primary motivation was to confirm the existence of a longitudinal-vortex secondary flow pattern for the flow over the relatively smooth-surfaced waves. We will focus on this aspect of the results in §6 but first present some cross-stream-averaged results.

The LES model runs to be presented are for a domain size of $2\lambda \times 2\lambda \times \lambda$, where λ is the wavelength of the waves. Thus the model domain covers two waves in the along-flow and cross-flow directions and extends to the top of the boundary layer (which is at a height of order λ) of the original wind tunnel experiment. The finite difference grid is uniform and isotropic with $128 \times 128 \times 64$ nodes. Periodic lateral boundary conditions are used and the spatial evolution of the wind tunnel flow is represented as temporal evolution in the LES, as described above in §2. At the bottom surface, the frictional momentum flux is computed locally from the horizontal velocity at the lowest grid cell assuming a logarithmic wind profile for a rough surface with a given roughness length z_0. The top boundary is rigid and impermeable ($w = 0$) but free slip and stress free ($\partial U/\partial z = 0$). The subgrid-scale (SGS) fluxes are determined by means of an eddy diffusivity which is a function of the grid scale and the SGS kinetic energy, which is itself computed from a separate transport equation. The flow is forced by a mean horizontal pressure gradient, which is determined such that the mass flux through the domain stays constant (Dörnbrack & Schumann 1993). Initial conditions were chosen to match the upstream flow in the wind tunnel. For further details of the LES model and its numerical implementation see Krettenauer & Schumann (1992) and Maas & Schumann (1994).

The wind tunnel flow between wave crests 11 and 12 was found to be best represented (based on boundary-layer depth) by the LES results for $t = 16T_{ref}$ (where $T_{ref} = \lambda/U_0$). Figure 9 shows results for the mean downstream velocity profiles at crest, trough and intermediate locations for both relatively smooth- and rough-wave experiments. The mean values were obtained by averaging the field over the cross-stream direction and over positions (2) of equal phase of the orographic waves within the computational domain. This was at a single value for time ($16T_{ref}$) and involved averaging over 256 individual values to obtain a mean. Ideally we would have also averaged over a number of realizations of the flow, perhaps with slight perturbations to the initial conditions, but this was not done. However we did check mean profiles at other times ($14T_{ref}$, $15T_{ref}$, $17T_{ref}$, $18T_{ref}$). These always showed very similar overall profiles (in x or z) to those at $t = 16T_{ref}$ but the fine-scale details of the profile were often slightly different. Initial normalization within the model was with respect to a bulk velocity. Plotted results are re-scaled to the local velocity at the model top. The general features of the wind tunnel data (the S-shape of the crest profiles, the height of the crossing point between the profiles of $x = 0.25\lambda$ and $x = 0.75\lambda$) are represented quite well by the LES. In figure 9(*a*) profiles at the trough and halfway down the slope for the smooth case fit the experimental data very well. Starting at $t = 4T_{ref}$ the mean profiles show positive U-values for all locations and there is no steady recirculation zone. Recirculations only occur locally and temporarily in very small areas near the

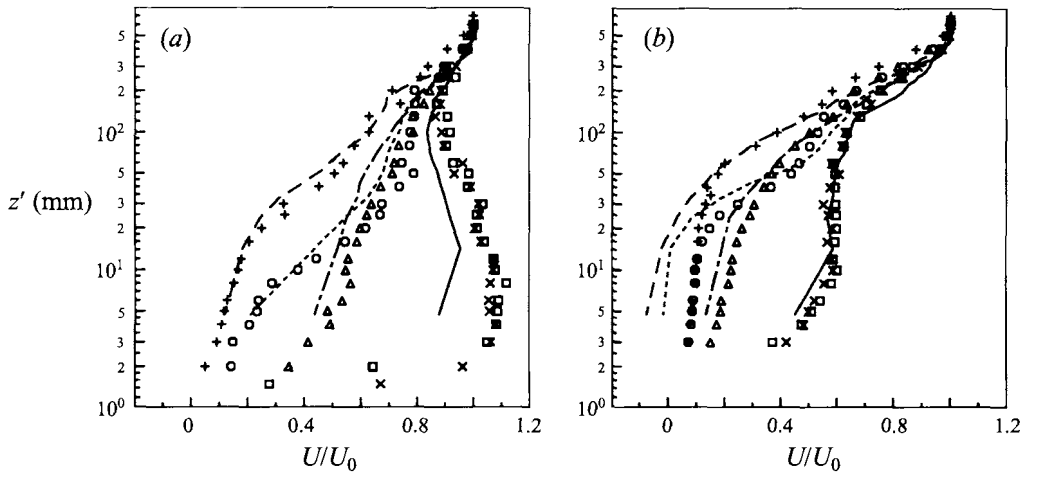

FIGURE 9. Mean velocity profiles, U/U_0 *vs.* $\log z'$, from the LES at locations between the wave crests at $t = 16T_{ref}$, compared to the wind tunnel data from figure 5: (*a*) smooth waves, (*b*) rough waves. Solid lines are for profiles above the crests, short-dashed lines at locations 1/4 wavelength downstream of the crests, long-dashed lines represent the mean profile above the troughs and long–short-dashed lines are the profiles 3/4 of a wavelength downstream of the crests.

Surface type	$\langle\tau_{fric}\rangle$	F_p	$\langle\tau_{fric}\rangle + F_p$
Rel. smooth	0.0020	0.0027	0.0047
Rel. rough	0.0016	0.0054	0.0070

TABLE 2. Drag values over the waves: LES results. All drag values are per unit area and are normalized by ρU_0^2. They are based on LES results at $t = 16T_{ref}$: $\langle\tau_{fric}\rangle$ is horizontal force on the surface due to friction, F_p is normalized form drag, calculated from (4)

surface downstream of the crest. The crest and halfway-up profiles have slightly lower mean velocity values for the near-surface layer ($z \leqslant 100$ mm) than were measured in the wind tunnel. Besides problems of insufficient resolution near the surface (see discussion below) the systematic lateral variation in the time-averaged wind tunnel velocity data due to three-dimensional flow structures may have caused the discrepancy since an average taken over y can be different from the profile at any y-location. The extreme instantaneous LES velocities at $z' = 5$ mm above the crest were $U_{max} = 1.40$ and $U_{min} = 0.75$. There is generally an organization into narrow high-speed regions, or streaks, surrounded by broader areas of lower velocity, and the range of simulated profiles easily spans the experimental data. These were from the tunnel centreline and, as will be shown later, correspond to higher speeds than were found to either side. The agreement is far better than that obtained with a model based on the Reynolds-averaged equations (Taylor *et al.* 1995).

In the rough case the agreement between LES and measured results for the crest profile is better (Figure 9*b*). There are steady recirculation zones downstream of the crests and mean velocities are negative up to a height z' of about 20 mm in the trough. This recirculation was qualitatively observed in the experiment but the hot-wire anemometer was unable to differentiate between positive and negative quantities.

The surface pressure distributions at $t = 16T_{ref}$ for both runs are shown in figure 6(*a*) and the calculated surface fluxes are listed in table 2. The plotted pressure results are

again averages over y and at two locations with the same phase. Results for $t = 14T_{ref}$, $15T_{ref}$, $17T_{ref}$ and $18T_{ref}$ were again similar but with differences in fine detail (e.g. the 'kink' in the rough-wall pressure plot at about $x/\lambda = 0.1$ is smoother at $15T_{ref}$ than at $16T_{ref}$). The surface pressure distributions appear to agree well with the experimental results in general. The slightly weaker pressure minimum over the crest in the relatively smooth-wall LES results compared to the wind tunnel measurements is qualitatively consistent (through Bernoulli's equation) with the lower LES velocities over the crest discussed above. There are some systematic differences between the wind tunnel and LES pressures on the downstream side of the crest ($0 \leqslant x/\lambda \leqslant 0.5$). In the relatively smooth-surface case the LES pressures are higher than the wind tunnel values in the vicinity of $x/\lambda = 0.8$. These lead to lower pressure differences across the crest and a significantly lower form drag as can be seen from a comparison of tables 1 and 2. In the rough case there is again good agreement except that the LES pressure minimum over the crest ($x = 0$) is slightly deeper than the observed value. There are other small differences and the LES form drag is slightly lower than that calculated from the wind tunnel pressures. The LES ($\langle \tau_{fric} \rangle$) and wind tunnel ($\langle u_*^2 \rangle$) shear stress contributions are in reasonable agreement, and both have lower values in the rough case.

It is clearly rather anomalous that the wind tunnel observations (table 1) indicate higher form drag for the attached flow over the relatively smooth-surfaced wave than for the separated flow over the rough wave while the LES results (table 2) indicate the opposite. It would be highly desirable to see the wind tunnel measurements repeated in another facility and to see similar measurements for a wider range of wave steepness and λ/z_0 values. Models based on the use of Reynolds-averaged equations also have considerable uncertainty in their predictions of form drag. Ayotte *et al.* (1994), Wood & Mason (1993) and Xu *et al.* (1994) all make the point that form drag predictions are strongly dependent on the turbulence closure assumptions made in these models. It would appear from the present results that there are also difficulties with LES and wind tunnel determinations of this very sensitive, but important, flow statistic.

It is a general characteristic of LES atmospheric boundary-layer models that they perform well in convective situations where large eddies dominate and are more temperamental, and more sensitive to subgrid-scale parameterizations, in the simulation of neutral and stably stratified flows (Mason 1994). Although our flow is neutrally stratified, we expect the presence of the wavy topography to generate large-eddy structures and anticipated that a LES model would perform well for this flow. The results confirm this although there is considerable variation of some sensitive model output parameters, e.g. the form drag, between runs with different resolution, with non-uniform grids, modified finite differences or with different initial conditions.

The resolution problem is associated, at least in part, with our inability to resolve the very thin shear layer with the large shear stress gradient above the wave crests. This has a thickness of order 3 mm while the boundary-layer depth is 600 mm. With our choice of $N = 64$ grid points in the vertical direction, the lowest grid is at $\Delta z/2 \approx 0.008H$, or approximately 5.0 mm. This means that with $N = 64$ we do not resolve the inner layer but parametrize it in terms of the logarithmic wind profile. Adequate resolution, with a uniform isotropic three-dimensional model would require of order $512 \times 512 \times 256$ grid nodes. Further development of LES models including better treatment of near-wall layer, or bigger faster computers may resolve these difficulties but for the moment we will regard our LES results as good qualitative simulations of the wind tunnel flow without expecting exact quantitative agreement.

6. Secondary flow

The primary wind tunnel evidence of secondary flow arose when we set out to check that the flow over the two-dimensional waves was itself two-dimensional and laterally uniform, at least over the central portion of the tunnel. Somewhat to our surprise and initial dismay we discovered that, in the relatively smooth-surface study, there were lateral (y) variations, at about the $\pm 5\%$ level, in the mean velocity values at fixed x and z locations. To the best of our knowledge these have not been reported in any previous studies of flow over wavy surfaces. The lateral variability was absent in the upstream flow and in the flat-floor tests and we believe that it is associated with an instability of the two-dimensional flow over the waves leading to the establishment of a secondary flow comprised of longitudinal vortices. Our initial thoughts were that this could be a Görtler (1940) instability (or centrifugal instability) associated with streamline curvature in the troughs but the vertical extent of the secondary flow is rather large for this. J. C. R. Hunt (personal communication) and Hunt *et al.* (1991) suggest that it may be a novel form of Langmuir circulation (see Craik 1982). This is also indicated by the recent work of Phillips & Wu (1994) on the development of longitudinal vortex modes in inviscid linear shear flow through the Craik–Leibovich type-2 instability and by subsequent work by W. R. C. Phillips and collaborators (personal communication) on the inviscid and viscous instability of power-law and logarithmic velocity profiles to spanwise-periodic longitudinal vortex modes. So far we have been unable to establish the necessary theoretical details and in this section will present only the experimental observations and LES results which indicate somewhat similar, though not identical, features. In an unbounded two-dimensional flow situation the three-dimensional structures would probably meander laterally and be averaged out in any long period measurement. In the wind tunnel the sidewalls constrain this meandering and cause lateral variability in the time-averaged flow.

As our check for two-dimensionality of the mean flow, lateral traversing measurements were made to 900 mm on each side of the centreline of the wind tunnel, the maximum lateral coverage allowed by the traverse facility, at several heights and at several downstream locations. Figure 10 shows selected plots from a series of transverse profiles of the mean velocity over the smooth waves. The flow was reasonably homogeneous in the spanwise direction at the upstream reference position (1.3 m or just over 2λ upstream of the leading edge of the waves); there were small variations, of about $\pm 2\%$, in the mean velocity but no recognizable patterns. The lateral variability was still small over the first crest (figure 10*a*) but in the first trough, substantial three-dimensional disturbances (spanwise variations) start to occur at low levels ($z' = 20$ mm). These disturbances persist and could be seen at the subsequent measurement locations (i.e. the second and the fourth crests, the 11th trough and the 12th crest). The spanwise variations of the mean velocity over the waves are well organized in a wavy, or a W-shaped pattern with two minima located roughly 400 mm off the centreline on each side. This is well illustrated by the results for $z' = 100$ mm over the 11th trough and 12th crest (see figure 10*b*, *c*). The effective wavelength of the disturbances is about 800 mm which is comparable with both the model wavelength and the boundary-layer depth over the waves. The disturbances are confined within the boundary layer, as illustrated by our measurements at $z' = 600$ mm over the 12th crest, and, once established, grow in depth together with the boundary layer. To evaluate the development of the three-dimensional disturbances over the waves, the range of the spanwise variation in the central part of the tunnel, $|Y| \leqslant 600$ mm, normalized by the free-stream velocity was determined. The intensity of the disturbance was found to

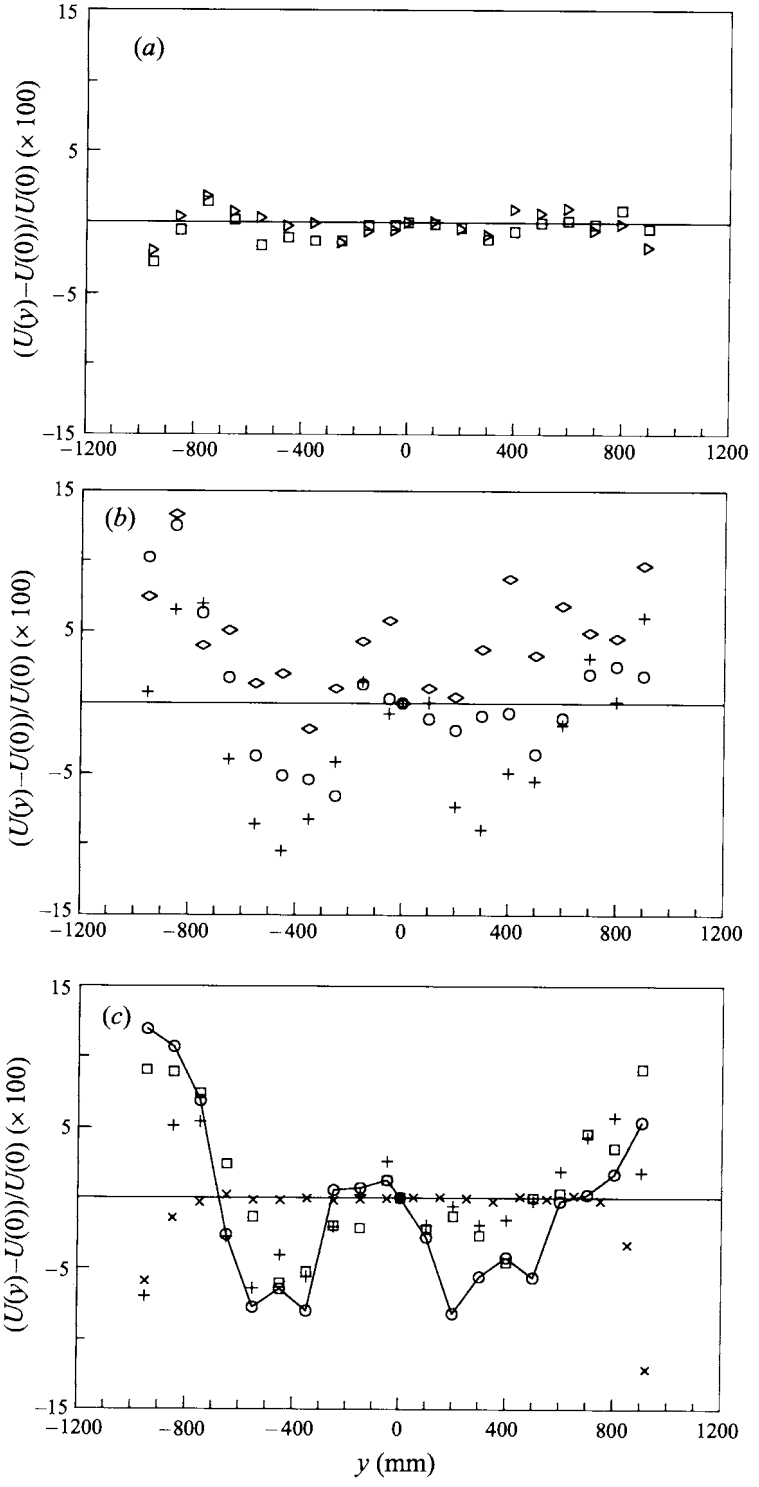

FIGURE 10. Wind tunnel measurements of the lateral (y) variation of mean velocity $(U(y)-U(0))/U(0)$ over the smooth-wave model at fixed x and z', $U(0)$ is the value at the tunnel centreline, $y = 0$: (*a*) first crest; (*b*) 11th trough; (*c*) 12th crest. Heights, z' (in mm) for the measurements are ▷, 5; ◇, 10; □, 20; ○, 100; +, 300; ×, 600.

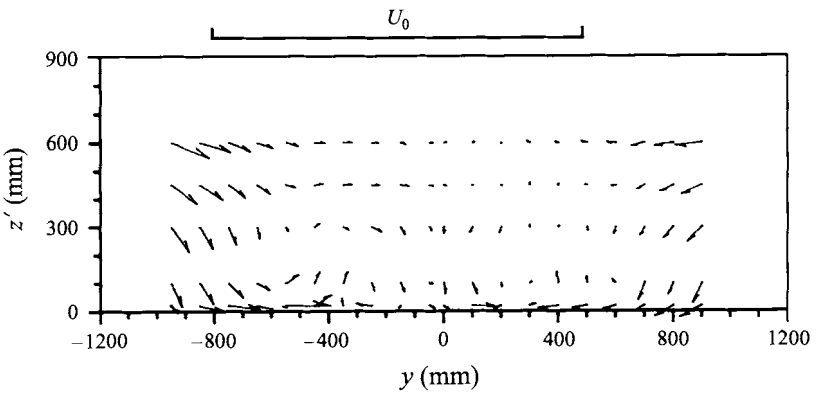

FIGURE 11. Vector plot of secondary flow (V, W) over the 12th crest (relatively smooth-surface case). Horizontal scale above the figure represents U_0 (approximately 10 m s^{-1}).

grow rapidly over the first few waves and then appeared to saturate at a range of about $0.1U_0$ in the central part of the wind tunnel, although there were differences between crest and trough ranges and larger variations as the sidewalls were approached.

The three-dimensional disturbances could also be seen in the turbulence field over the waves. The percentage spanwise variation in σ_u was similar to that of the mean velocity but with opposite sign and was less organized than in the mean flow, especially in the troughs. Some tests were carried out over the smooth waves with different wind tunnel speeds, 15, 5 and 2.5 m s^{-1}, to determine whether the three-dimensional disturbances over the waves are dependent on Reynolds number. The measurements show that, when U_0 is greater than 10 m s^{-1}, the primary two-dimensional flow over the waves is Reynolds-number independent and so are the three-dimensional disturbances. However, when U_0 is less than 10 m s^{-1}, the flow over the waves is Reynolds-number dependent, although the upstream flow over the flat floor is independent of Reynolds number, and the three-dimensional disturbances behave differently for different wind tunnel speeds. For example, with $U_0 = 5$ m s^{-1}, the spanwise variation shows only a single trough, i.e. a V-pattern, over the second crest and a widened trough over the 12th crest, while, with $U_0 = 2.5$ m s^{-1}, the disturbances start with the W-pattern but end up with a single trough over the 12th crest.

For the high wind speeds we speculate that the wavy pattern of the spanwise variation of the flow over the smooth waves could be associated with longitudinal vortices, and further measurements with X-wire probes were made to obtain the V- and W-components of the mean flow. Figure 11 is a vector plot of the secondary flow constructed from a series of these measurements over the 12th crest. There are clearly limitations to our study caused by the limited width of the wind tunnel and sidewall effects, and corner vortices may well be influencing or modifying the secondary flow pattern. However, in figure 11 one can tentatively identify two pairs of counter-rotating vortices over the waves. Descending flow is found at the centre and close to the sidewalls causing horizontal divergence at the surface and bringing fluid with relatively low turbulence from higher to lower levels, while ascending flow is found in between, about 400 mm off the centreline on each side. This description is consistent with the spanwise variations of the mean flow and turbulence described above and we believe this to be the most plausible explanation of our observations.

Previous studies on three-dimensional structure in primarily two-dimensional turbulent flow, for both spanwise vortical flow and the flow over concave walls, have

all noticed the dependence of the final three-dimensional structure on the upstream flow conditions. Lasheras, Cho & Maxworthy (1986) showed that, by removing disturbances from the upstream flow, the roll-up flow (of Kelvin–Helmholtz waves) could be free of three-dimensionality for some distance downstream, while, if a single localized perturbation was added to the upstream flow, that perturbation was then stretched and amplified by the positive strain of the spanwise vortices (roll-up) and also spread sideways, soon causing the formation of streamwise counter-rotating vortices. Swearingen & Blackwelder (1986) studied the spacing of the streamwise vortices over concave walls under various upstream conditions. They found that there was a natural wavelength for the spanwise variation which was independent of the downwind distance. When the disturbances introduced upstream (either at the end of the contraction or at the beginning of the concave curvature) had wavelength greater than the natural wavelength, the spacing of the longitudinal vortices was not affected, but, when the spanwise disturbances introduced had wavelengths smaller than the natural one, the vortex spacing downstream corresponded to the wavelength of the introduced disturbances. However, the investigation was carried out at a fixed downwind location, and whether those altered vortex spacings would change further downstream was not indicated.

In the present study, the effect of upstream flow conditions on the disturbances over the waves was investigated for the smooth case only. First, we searched for possible sources of upstream disturbances to the flow with the same spanwise wavelength as the perturbations. Finding none, we introduced small perturbations upstream of the honeycomb to see if these had any impact and discovered that they did not. Upstream disturbances were then introduced by vortex generators (pairs of half-delta wings angled to the flow, similar to those used by Hoffmann, Muck & Bradshaw 1985, with length 160 mm and a height, or span, of 40 mm), located with their trailing edges 3.66 m upstream of the start of the waves. Two sets of measurements, were made with ten pairs and six pairs of vortex generators evenly spaced across the tunnel floor, respectively.

With ten pairs of vortex generators, ten pairs of counter-rotating vortices appeared to form (eight clearly seen and the two outer ones beyond our lateral measurement range) at the upstream reference location (2.3 m from the trailing edge of the generators) over the flat floor. The vortex structure remained similar over the first crest although attenuated. Over the first trough and the second crest, the pattern of the spanwise variation was still essentially the same as upstream although with some deformation especially at the lower level in the trough. Then, although ten pairs of longitudinal vortices were still recognizable at the higher level over the fourth crest, the number of vortex pairs was reduced at the lower level. Farther downwind, over the 12th crest, the spanwise disturbance was dominated by about three pairs of streamwise vortices at all levels within the boundary layer. There were certainly quantitative differences between this plot and the results shown in figure 12 but the overall pattern was similar. At this stage the spanwise wavelength of the secondary flow appeared to be about 600 mm compared to 800 mm in the original case. The results with six pairs of upstream vortex generators were basically the same, and, although six vortex pairs could still be identified over the second crest, the profile was clearly deformed by some larger-scale perturbations and, over the 12th crest, the spanwise variation had a wavelength of order 800 mm and was almost identical to that without upstream vortex generators.

The above discussion suggests that, in our flow situation, the scale of the disturbances over the waves is determined by a flow instability. There is undoubtedly

a sidewall effect as well, since the sidewalls provide lateral constraints. Disturbances in the upstream flow may be amplified or damped selectively according to the natural wavelength of the flow instability, but appear to have no direct control of the final pattern of the three-dimensional structure over the waves.

We also measured lateral profiles for the 11th trough and 12th crest over the rough (carpeted) waves. As discussed above, changing the surface roughness led to considerable differences in flow separation, speed-up over the crests and vertical velocity shear. Over the rough waves the spanwise variations show lower velocities in the central part of the tunnel over both the crest and trough and quite large increases near one wall. Vector plots for the secondary flow were produced but there were no clear signs of longitudinal vortices over the rough waves. We tentatively suggest that no organized three-dimensional structures develop in the rough-wall case and that the velocity increases for $|Y| \geqslant 600$ mm are linked to sidewall and corner vortex effects.

The secondary flow observations are less complete than we would have liked and there is clearly a need to undertake further investigation. The similarity in scale between the wavelength and the boundary-layer depth is unfortunate and measurements in a deeper boundary layer would be desirable. It would also be interesting to explore a range of flow parameters $(\lambda/z_0, ak)$ to determine how common the occurrence of the secondary flow might be and how they might affect the scales of the secondary three-dimensional structure. As far as we are aware it has not been observed in the other studies of flow over sinusoidal waves discussed above, but lateral variability checks are not reported and may not have been made.

Turning to the occurrence of organized three-dimensional flow structures in the LES results, figure 12(*a*) shows the spanwise variation of the instantaneous velocity field (v, w) at $t = 16T_{ref}$ in (Y, Z)-planes at five x-locations covering one wavelength in the relatively smooth-surface case. The mean flow is out of the plane of the figures. Over the crest at $x = -\lambda$ (figure 12*a*i) the flow is accelerated in the streamwise direction, the lateral (v, w) velocities are relatively small and no coherent structures are clearly detectable in the near-surface region. It is however apparent that there are areas of ascent (near $y/\lambda = -0.95$, -0.5 and 0.3) and strong near-surface descent (near $y/\lambda = -0.75$ and 0.95). This seems to evolve into some organized flow structure in the trough position at $x = -0.5\lambda$ (figure 12*a*iii) where two pairs of counter-rotating vortices can be clearly identified. Their centres are at a height of approximately 0.2λ and the y/λ locations of the vortex centres are approximately -0.85, -0.65 and 0.5, 0.9. The vortices have a typical lateral and vertical extent of order $\lambda/3$, with part of the channel cross-section occupied by relatively unstructured flow. At the next crest (figure 12*a*v) the vortices are somewhat suppressed but there are again reasonably well-defined areas of near-surface ascent and descent. Stronger vortical structures were again apparent in the following trough ($x/\lambda = 0.5$).

In figure 12(*b*), for flow over the rough-surfaced waves, one strong vortex is visible over the trough (centred at $y = -0.9\lambda$, $z' = 0.2\lambda$, figure 12*b*iii), but the general flow characteristics are different from the relatively smooth case. Owing to the rougher surface, large separated regions exist downstream of each crest. In these zones circulations with axes parallel to the crest dominate and cause a very turbulent flow with strong lateral variations in the velocity field. This is especially noticeable in plots of (v, w) at intermediate locations between the crests and troughs (figure 12*b*ii, iv) where the flow does not follow the orography in downward and upward motion (in comparison with the smooth case, figure 12*a*ii, iv) but shows pronounced turbulent flow in the spanwise direction.

The perturbation vertical velocity field at $T = 16T_{ref}$ for the computational level

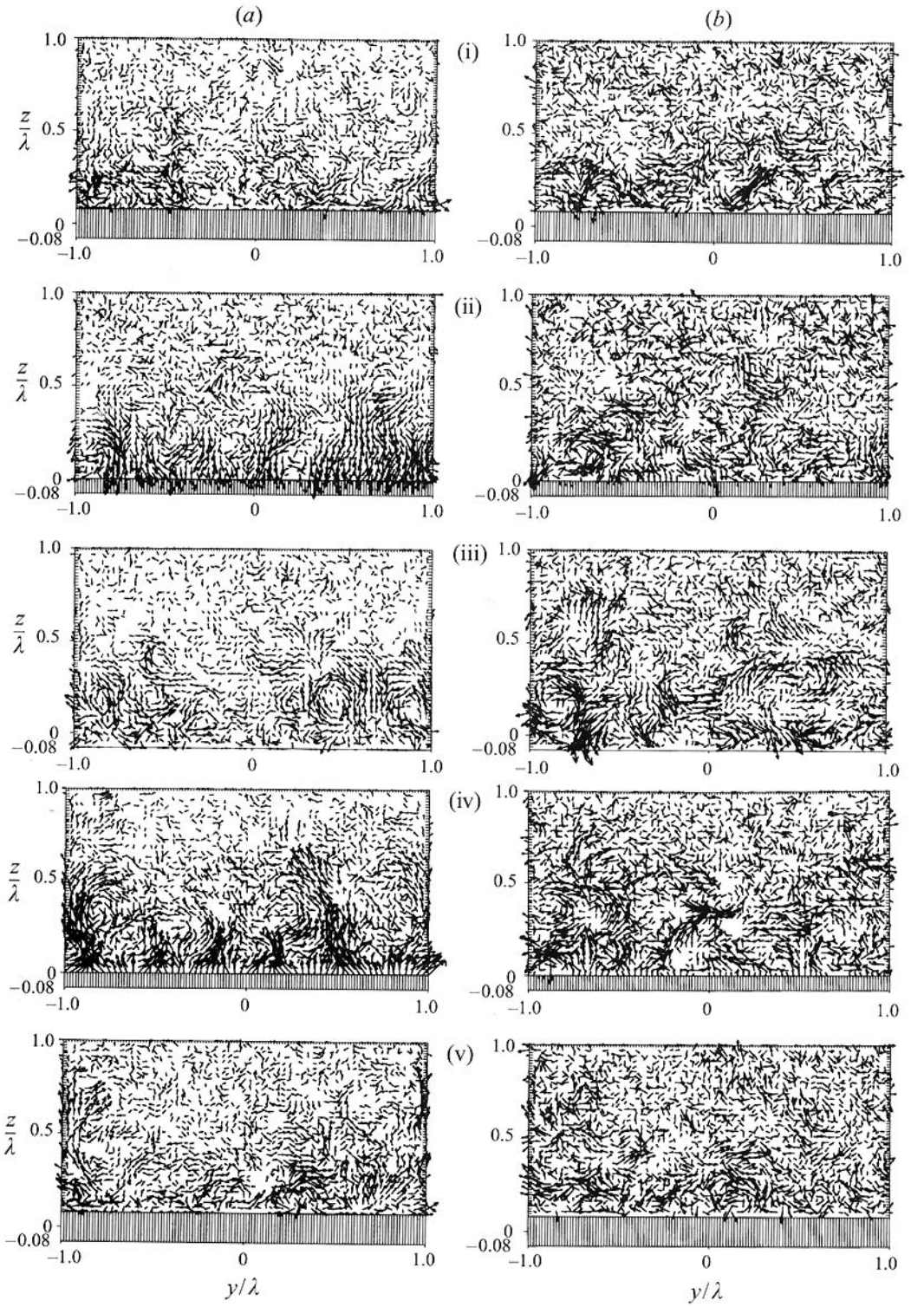

FIGURE 12. Instantaneous (V, W) velocity vectors from the LES for (a) the relatively smooth-surfaced case and (b) the rough-surfaced case at time $t = 16T_{ref}$ for different x locations: (i) $x = -\lambda$ (crest); (ii) $x = -0.75\lambda$ (downslope); (iii) $x = -0.5\lambda$ (trough); (iv) $x = -0.25\lambda$ (upslope); (v) $x = 0.0\lambda$ (crest). These plots use z, rather than z' as the vertical coordinate and the shaded (lined) areas lie below the wave.

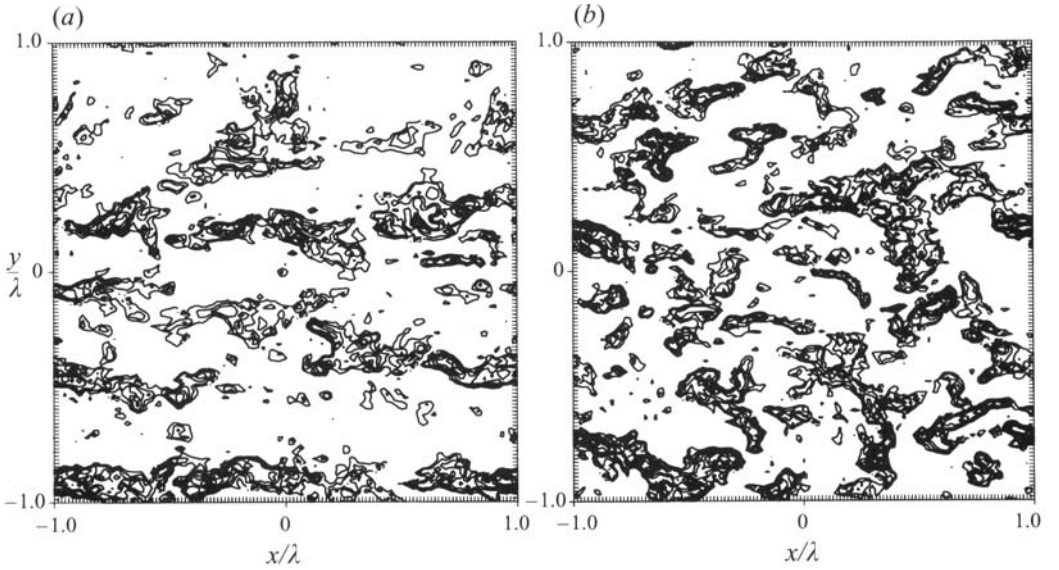

FIGURE 13. LES vertical velocity variations (w') relative to y-average value at $t = 16T_{ref}$, $\eta = 0.11\lambda$. (*a*) Relatively smooth-surfaced waves, (*b*) relatively rough-surfaced waves. Positive contours only, the contour interval is $0.05U_0$.

$\eta = 0.11\lambda$ is shown in figure 13. The perturbation field is used to eliminate the terrain-following contribution to W and is defined by $w' = W - \langle W \rangle_y$ where $\langle W \rangle_y$ is the lateral average, with respect to y, of W at fixed, x, z and t. This statistic will highlight longitudinal vortices but will eliminate transverse vortex structures with axes in the y-direction. Only positive values are plotted to illustrate the vortical structures, which are characterized by alternating regions of positive and negative w'. It is clear from a comparison between the plots for the relatively smooth- and rough-surfaced waves that organized vortices aligned with the flow are present in the smooth case but are less ordered over the rough surface. They appear to be less persistent than the structures we anticipated based on the wind tunnel observations and they do meander laterally, but they are there. At most of the x-positions there are four regions of positive velocity, indicating four pairs of vortices with a lateral width of 0.25λ. Similar plots were produced for other levels. Close to the surface ($\eta = 0.02\lambda$) there was more small-scale structure in the w' fields while the fields at $\eta = 0.2\lambda$ were similar to those for 0.11λ.

Going back to the lateral variations of U which had initially alerted us to the existence of the secondary flow in the wind tunnel, we plotted lateral profiles of the instantaneous perturbation u velocity, $u' = u - \langle u \rangle_y$, at $t = 16T_{ref}$ at various x and z locations in the flow over the relatively smooth wall. The instantaneous LES u values show both secondary flow and turbulent fluctuations, if indeed it is appropriate to make such a distinction, while the wind tunnel data (figure 10) are time averages. In an attempt to remove some of the high-frequency turbulent fluctuations some smoothing in y (a three-point filter applied three times) has been conducted and selected results are shown in figure 14. Because of unconstrained 'meandering' by any secondary flow structures in the LES case (no boundary walls) long time averaging would eliminate both turbulence and secondary flow variations. The magnitudes of the lateral u' variations in these LES results for the relatively smooth-surfaced waves are roughly double the time-averaged wind tunnel values. This could be partially due to the effect of limited meandering in the wind tunnel. Subjective interpretation of the results

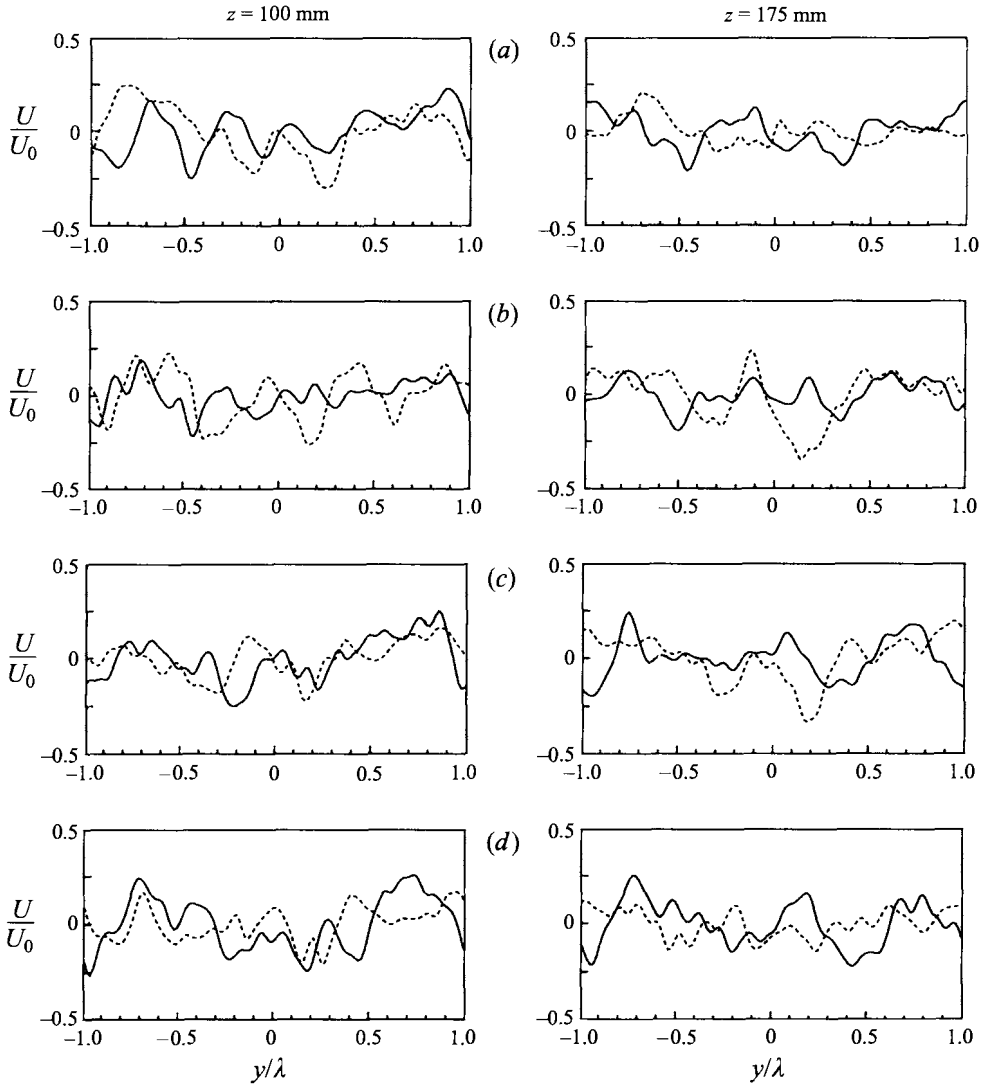

FIGURE 14. Sample LES lateral variation of instantaneous but spatially (y) smoothed u-component perturbation velocity above (a) wave crests $x = -\lambda$, 0; (b) mid-slope locations $x = -0$, 75λ, 0.25λ; (c) troughs $= -0.5\lambda$, 0.5λ and (d) mid-slope locations $x = -0.25\lambda$, 0.75λ, for $t = 16T_{ref}$ at selected η levels (100 and 175 mm). Results for relatively smooth-surfaced waves. Solid lines correspond to the field over the first wave ($-\lambda < x < 0$) and the dashed lines to the second wave ($0 < x < \lambda$).

in figure 14 suggests some loose similarity between the low-wavenumber variations in figure 14(a, c) and the wind tunnel plots of figure 10(c, b). With a little imagination we can 'see' three broad maxima in $u'(y)$ in many of the 'profiles' and there is a measure of consistency in the y location of these maxima at different x and z' positions. In both the wind tunnel and the LES results, the high u' values correspond approximately to downwelling motions while u' minima appear to be associated with upwelling regions in figures 11 and 12(a). The LES results are less compelling than figure 10 but can be interpreted as indicating a persistent and somewhat wave-like pattern which has features in common with the wind tunnel study.

Overall we can see some measure of qualitative agreement with the secondary flow detected in the wind tunnel experiment and the vortex structures present in the large-eddy simulations. Because of differences in flow situation, including the different impact of the sidewalls in the wind tunnel and the lateral periodic boundary conditions in LES, the agreement is far from perfect. However the primary intent of the LES runs was to support our hypothesis that there is a three-dimensional instability in the flow over the relatively smooth-surfaced waves which leads to the establishment of longitudinal vortex structures. We contend that the LES results support this interpretation of the wind tunnel data.

7. Conclusions

We have presented new results from a wind tunnel study of turbulent boundary-layer flow over wavy surfaces. The waves had a maximum slope of 0.5 and two different surface roughnesses were used. Over the rougher surface the mean flow separated over each wave and was approximately two-dimensional. Over the relatively smooth surface it remained attached after the first wave but, after the first few waves, we observed a three-dimensional secondary flow. In this case there is also a pronounced low-level 'jet' above the crests. Large-eddy simulation results are also presented. These match the observations well and support our interpretation of the flow structure. In nature it is possible that the three-dimensional secondary flow may occur in the airflow over water waves.

The original intent of the wind tunnel study was to measure the form drag and total horizontal force on the waves. This was achieved but there are some uncertainties in the values, especially over the rougher surface where there is a 50 % difference between total stress measurements based on the form drag and friction velocity and the value obtained from an overall momentum budget. The LES results for shear stress at the surface are in reasonable agreement with the wind tunnel but the form drag prediction for the relatively smooth-surfaced waves is much lower than the measured value. The experiment and the LES results confirm the suspicion, based on other modelling studies, that accurate prediction of the drag over topography may be a rather difficult goal to achieve.

Hans Teunissen of the Atmospheric Environment Service gave considerable guidance and advice in the setting up of the experiment. We are most grateful to him and also to Karl Venek and Mohammed Shokr for their advice and practical assistance in the conduct of the wind tunnel study. One of us (W.G.) was the holder of an AES/NSERC research fellowship during the initial conduct of the wind tunnel work. We much appreciate the help and encouragement of Ulrich Schumann (DLR) without those support we would not have completed the LES part of the study.

REFERENCES

ABRAHAMS, J. & HANRATTY, T. J. 1985 Relaxation effects over a wavy surface. *J. Fluid Mech.* **151**, 443–455.

AYOTTE, K. W., XU, D. & TAYLOR, P. A. 1994 The impact of different turbulent closures on predictions of the mixed spectral finite difference model for flow over topography. *Boundary-Layer Met.* **68**, 1–33.

BANDOU, T. & MITSUYASU, H. 1988 The structure of turbulent air flow over a wavy wall, Part 2, *Rep. Res. Inst. for Appl. Mech. Kyushu University*, No 104, 13–34.

BEEBE, P. S. & CERMAK, J. E. 1972 Turbulent flow over a wavy boundary. *Tech. Rep.* 16, CER 71-72 PSB-JEC 44, Fluid Dynamics and Diffusion Laboratory, Colorado State University, Fort Collins, Colorado, USA.

BELJAARS, A. C. M., WALMSLEY, J. L. & TAYLOR, P. A. 1987 A mixed spectral finite difference model for neutrally stratified boundary-layer flow over roughness change and topography. *Boundary-Layer Met.* **38**, 273–303.

BRITTER, R. E., HUNT, J. C. R. & RICHARDS, K. J. 1981 Airflow over a two dimensional hill; studies of velocity speed-up, roughness effects and turbulence. *Q. J. R. Met. Soc.* **107**, 91–110.

BUCKLES, J., HANRATTY, T. J. & ADRIAN, R. J. 1984 Turbulent flow over large-amplitude wavy surfaces. *J. Fluid Mech.* **140**, 27–44.

CAPONI, E. A., FORNBERG, B., KNIGHT, D. D., MCLEAN, J. W., SAFFMAN, P. G. & YUEN, H. C. 1982 Calculations of laminar viscous flow over a moving wavy surface. *J. Fluid Mech.* **124**, 347–362.

CARRUTHERS, D. J. & HUNT, J. C. R. 1990 Fluid mechanics of airflow over hills: turbulence, fluxes and waves in the boundary layer. In *Atmospheric Processes over Complex Terrain* (ed. W. Blumen). AMS Meteorological Monographs, 23, no 45, pp. 83–107.

COUNIHAN, J. 1974 Flow over concatenated sinusoidal hills. *Central Elect. Res. Lab.*, UK. *Rep.* RD/L/N57/74.

COUNIHAN, J. 1975 Adiabatic atmospheric boundary layers: a review and analysis of data from the period 1880–1972. *Atmos. Environ.* **9**, 871–905.

CRAIK, A. D. D. 1982 Wave-induced longitudinal-vortex instability in shear flows. *J. Fluid Mech.* **125**, 35–72.

DÖRNBRACK, A. & SCHUMANN, U. 1993 Numerical simulation of turbulent convective flow over wavy terrain. *Boundary-Layer Met.* **65**, 323–355.

FINNIGAN, J. J. 1988 Air flow over complex terrain. In *Flow and Transport in the Natural Environment* (ed. W. L. Steffen & O. T. Denmead), pp. 183–229. Springer.

FINNIGAN, J. J., RAUPACH, M. R., BRADLEY, E. F. & ALDIS, G. K. 1990 A wind tunnel study of turbulent flow over a two-dimensional ridge. *Boundary-Layer Met.* **50**, 277–317.

GARRATT, J. R. 1992 *The Atmospheric Boundary Layer.* Cambridge University Press.

GENT, P. R. & TAYLOR, P. A. 1977 A note on 'separation' over short wind waves. *Boundary-Layer Met.* **11**, 65–87.

GONG, W. & IBBETSON, A. 1989 A wind tunnel study of turbulent flow over model hills. *Boundary-Layer Met.* **49**, 113–148.

GÖRTLER, H. 1940 Uber eine dreidimensionale Instabilitaet laminarer Grenzschichten an konkaven Waenden. *Nachr. Ges. Wiss. Goettingen, Math.-Phys.* Klasse, Neue Folge I, **2**, 1–26.

HOFFMANN, P. H., MUCK, K. C. & BRADSHAW, P. 1985 The effect of concave surface curvature on turbulent boundary layers. *J. Fluid Mech.* **161**, 371–403.

HSU, S.-T. & KENNEDY, J. F. 1971 Turbulent flow in wavy pipes. *J. Fluid Mech.* **47**, 481–502.

HUNT, J. C. R., TAMPIERI, F., WENG, W. S. & CARRUTHERS, D. J. 1991 Air flow and turbulence over complex terrain: a colloquium and a computational workshop. *J. Fluid Mech.* **227**, 667–688.

JACKSON, P. S. & HUNT, J. C. R. 1975 Turbulent wind flow over a low hill. *Q. J. R. Met. Soc.* **101**, 929–955.

KAIMAL, J. C. & FINNIGAN, J. J. 1994 *Atmospheric Boundary Layer Flows: their Structure and Measurement.* Oxford University Press.

KENDALL, J. M. 1970 The turbulent boundary layer over a wall with progressive surface waves. *J. Fluid Mech.* **41**, 259–281.

KLEBANOFF, P. S. 1955 Characteristics of turbulence in a boundary layer with zero pressure gradient. *NACA Rep.* 1247.

KRETTENAUER, K. & SCHUMANN, U. 1992 Numerical simulation of turbulent convection over wavy terrain. *J. Fluid Mech.* **237**, 261–299.

KUZAN, J. D., HANRATTY, T. J. & ADRIAN, R. J. 1989 Turbulent flows with incipient separation over solid waves. *Exps. Fluids* **7**, 88–98.

LASHERAS, J. C., CHO, J. S. & MAXWORTHY, T. 1986 On the origin and evolution of streamwise vortical structure in a plane, free shear layer. *J. Fluid Mech.* **172**, 231–258.

LAWSON, R. E. & BRITTER, R. E. 1983 A note on the measurement of transverse velocity fluctuations with heated cylindrical sensors at small mean velocities. *J. Phys.* E: *Sci. Instrum.* **16**, 563–567.

MAAS, C. & SCHUMANN, U. 1994 Numerical simulation of turbulent flow over a wavy boundary. In *Direct and Large Eddy Simulation* I (ed. P. R. Voke, L. Kleiser & J. P. Chollet), pp. 287–297. Kluwer.

MAAT, N. & MAKIN, V. K. 1992 Numerical simulation of air flow over breaking waves. *Boundary-Layer Met.* **60**, 77–93.

MASON, P. J. 1994 Large-eddy simulation: a critical review of the technique. *Q. J. R. Met. Soc.* **120**, 1–26.

MICKLE, R. E., COOK, N. J., HOFF, A. M., JENSEN, N. O., SALMON, J. R., TAYLOR, P. A., TETZLAFF, G. & TEUNISSEN, H. W. 1988 The Askervein hill project: vertical profiles of wind and turbulence. *Boundary-Layer Met.* **43**, 143–169.

MILES, J. W. 1957 On the generation of surface waves by shear flows. *J. Fluid Mech.* **3**, 185–204.

MOTZFELD, H. 1937 Die turbulente Strömung an welligen Wanden. *Z. Angew. Math. Mech.* **17**, 193–212.

NEWLEY, T. M. J. 1985 Turbulent airflow over hills. PhD thesis, University of Cambridge, UK.

PANOFSKY, H. A. & DUTTON, J. A. 1983 *Atmospheric Turbulence: Models and Methods for Engineering Applications.* Wiley.

PHILLIPS, W. R. C. & WU, Z. 1994 On the instability of wave-catalysed longitudinal vortices in strong shear. *J. Fluid Mech.* **272**, 235–254.

SHOKR, M. & TEUNISSEN, H. W. 1988 Use of hot-wire anemometry in the AES boundary-layer wind tunnel with particular reference to flow over hill models. *Res. Rep.* MSRB 88-9. AES, 4905 Dufferin Street, Downsview, Ontario, Canada.

STANTON, T., MARSHALL, D. & HOUGHTON, R. 1932 The growth of waves on water due to the action of the wind. *Proc. R. Soc. Lond.* A **137**, 283–293.

STULL, R. B. 1988 *An Introduction to Boundary-Layer Meteorology.* Kluwer.

SUTTON, O. G. 1953 *Micrometeorology.* McGraw Hill.

SWEARINGEN, J. D. & BLACKWELDER, R. F. 1986 Spacing of streamwise vortices on concave walls. *AIAA J.* **24**, 1706–1709.

TAYLOR, P. A. 1977*a* Some numerical studies of surface boundary-layer flow above gentle topography. *Boundary-Layer Met.* **11**, 439–465.

TAYLOR, P. A. 1977*b* Numerical studies of neutrally stratified planetary boundary-layer flow above gentle topography 1. Two-dimensional cases. *Boundary-Layer Met.* **12**, 37–60.

TAYLOR, P. A., MASON, P. J. & BRADLEY, E. F. 1987 Boundary-layer flow over low hills – A review. *Boundary-Layer Met.* **39**, 107–132.

TAYLOR, P. A., SYKES, R. I. & MASON, P. J. 1989 On the parameterisation of drag over small-scale topography in neutrally-stratified boundary-layer flow. *Boundary-Layer Met.* **48**, 409–422.

TAYLOR, P. A., XU, D., GONG, W. & AYOTTE, K. W. 1995 Modelling turbulent boundary-layer flow over 2D sinusoidal waves. *Proc. Intl Symp. on the Air–Sea Interface.* University of Toronto Press (to appear).

TEUNISSEN, H. W. & FLAY, R. G. J. 1981 Wind-tunnel simulation of planetary boundary-layer flow over an isolated hill: Part 1, rough model. *Rep.* MSRB 81-3. AES, 4905 Dufferin Street, Downsview, Ontario, Canada.

TOWNSEND, A. A. 1972 Flow in a deep turbulent boundary-layer over a surface distorted by water waves. *J. Fluid Mech.* **55**, 719–735.

WALMSLEY, J. L., SALMON, J. R. & TAYLOR, P. A. 1982 On the application of a model of boundary-layer flow over low hills to real terrain. *Boundary-Layer Met.* **23**, 17–46.

WOOD, N. & MASON, P. J. 1993 The pressure force induced by neutral, turbulent flow over hills. *Q. J. R. Met. Soc.* **119**, 1233–1267.

XU, D., AYOTTE, K. W. & TAYLOR, P. A. 1994 Development of the NLMSFD model of turbulent boundary-layer flow over topography. *Boundary-Layer Met.* **70**, 341–367.

XU, D. & TAYLOR, P. A. 1992 A non-linear extension of the mixed spectral finite difference model for neutrally stratified flow over topography. *Boundary-Layer Met.* **59**, 177–186.

ZILKER, D. P., COOK, G. W. & HANRATTY, T. J. 1977 Influence of the amplitude of a solid wavy wall on a turbulent flow. Part 1. Non-separated flows. *J. Fluid Mech.* **82**, 29–51.

ZILKER, D. P. & HANRATTY, T. J. 1979 Influence of the amplitude of a solid wavy wall on a turbulent flow. Part 2. Separated flows. *J. Fluid Mech.* **90**, 257–271.